Magnetic Reconnection

A. Bhattacharjee

Center for Heliophysics

Department of Astrophysical Sciences

Princeton Plasma Physics Laboratory

Princeton University

LWS Heliophysics Summer School, July 23-July 30, 2019

What is Magnetic Reconnection?

If a plasma is perfectly conducting, that is, it obeys the ideal Ohm's law,

$$E + v \times B = 0$$

B-lines are frozen in the plasma, and no reconnection occurs.

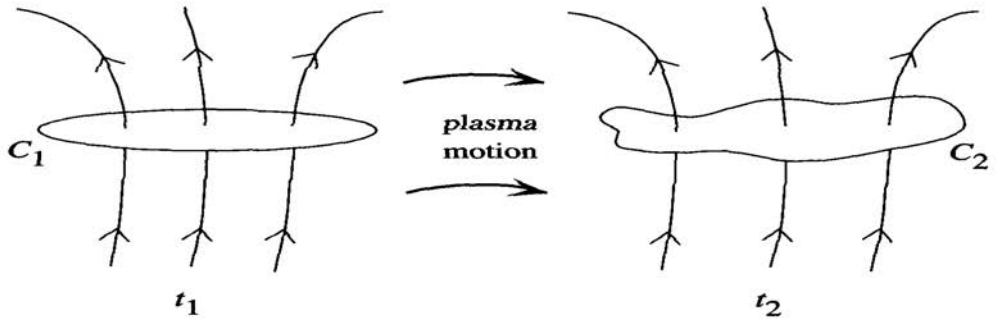

Fig. 1.6. Magnetic flux conservation: if a curve C_1 is distorted into C_2 by plasma motion, the flux through C_1 at t_1 equals the flux through C_2 at t_2.

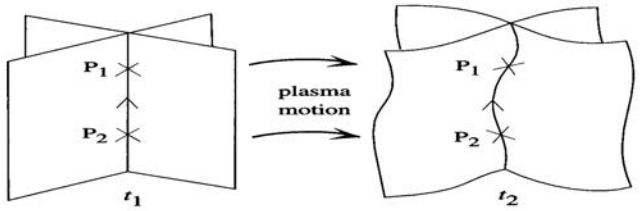

Fig. 1.7. Magnetic field-line conservation: if plasma elements P_1 and P_2 lie on a field line at time t_1, then they will lie on the same line at a later time t_2.

Magnetic Reconnection: Definition

Departures from ideal behavior, represented by

$$E + v \times B = R, \quad B \cdot \nabla \times R = 0$$

break ideal topological invariants, allowing field lines to break and reconnect.

In the generalized Ohm's law for weakly collisional or collisionless plasmas, **R** contains resistivity, Hall current, electron inertia and pressure.

Magnetic Reconnection

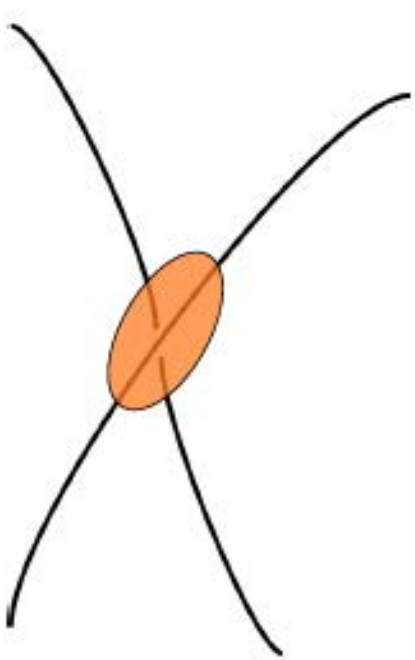

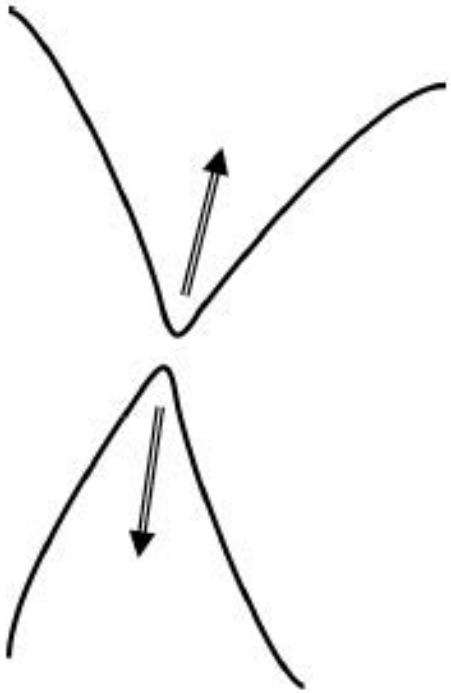

Before reconnection ***After reconnection***

- **Topological rearrangement of magnetic field lines**
- **Magnetic energy => Kinetic energy**

Example of Topological Change: Magnetic Island Formation

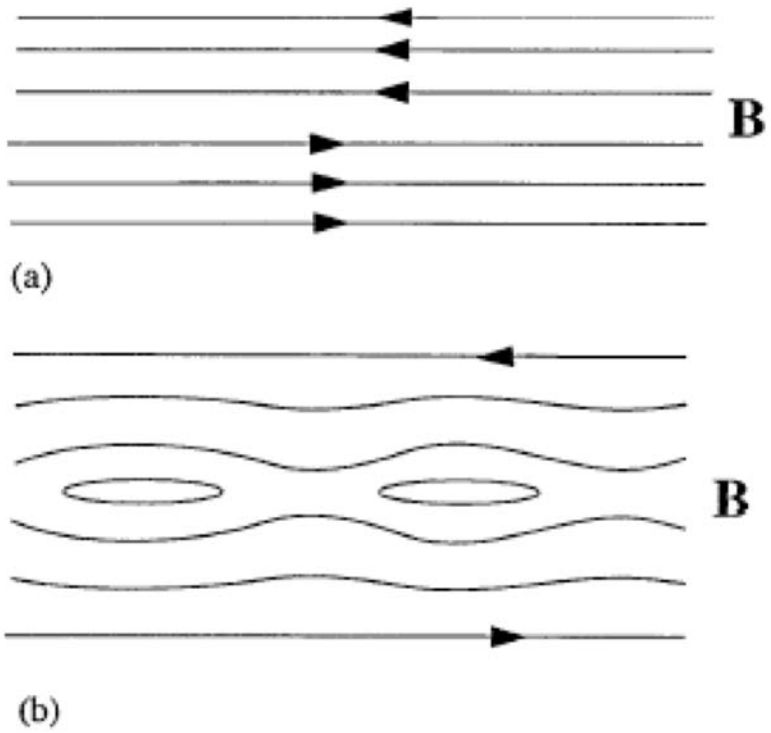

FIG. 1. (a) The topology of field lines in the Harris equilibrium $\mathbf{B}=B_0 \tanh(z/a)\hat{\mathbf{x}}$. (b) The topology of field lines when the perturbation $\mathbf{b}=b \sin(kx)\hat{\mathbf{z}}$ is imposed on the Harris equilibrium.

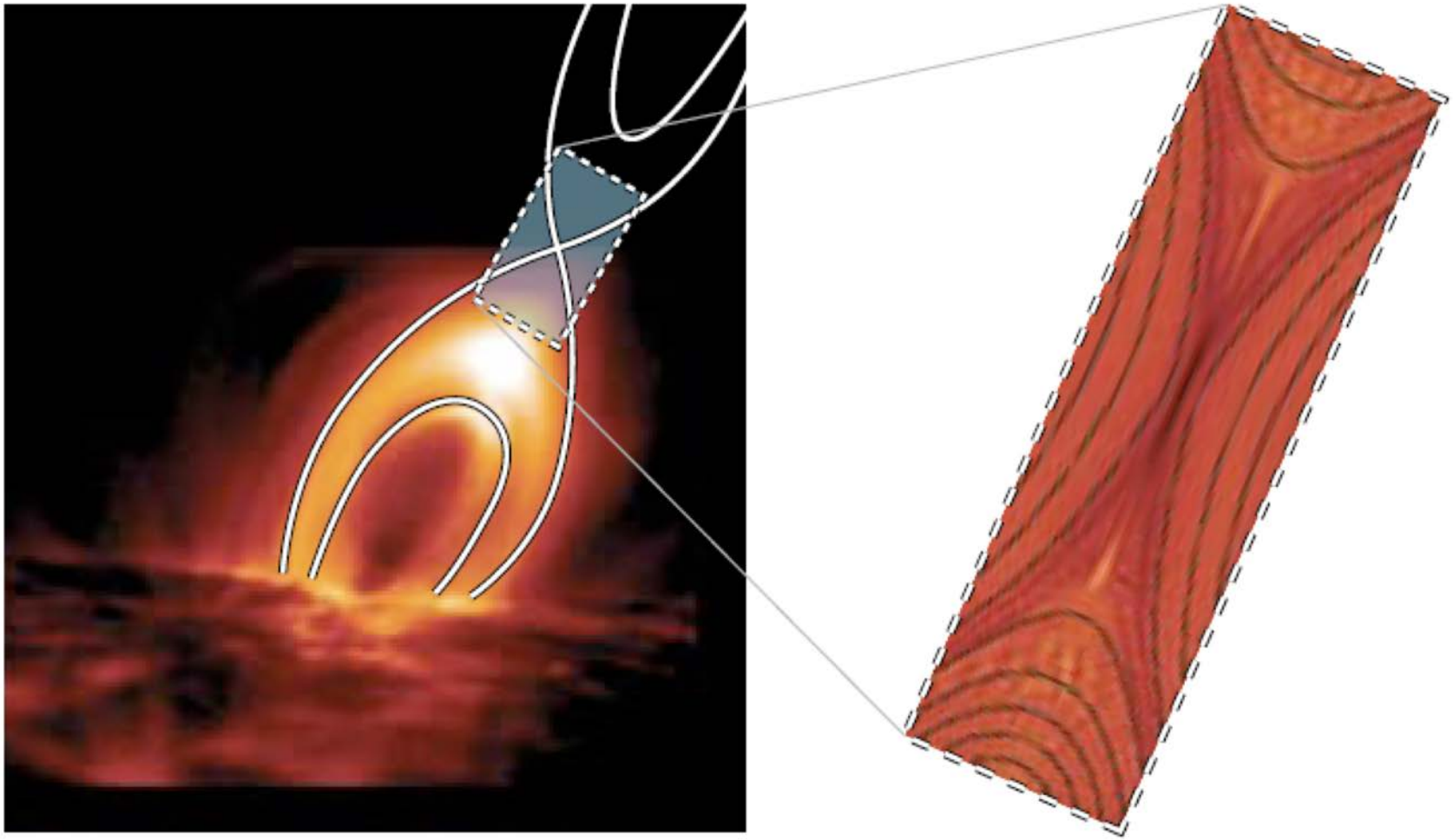

Courtesy: J. Burch and J. Drake, MMS Mission

The Flaring Sun

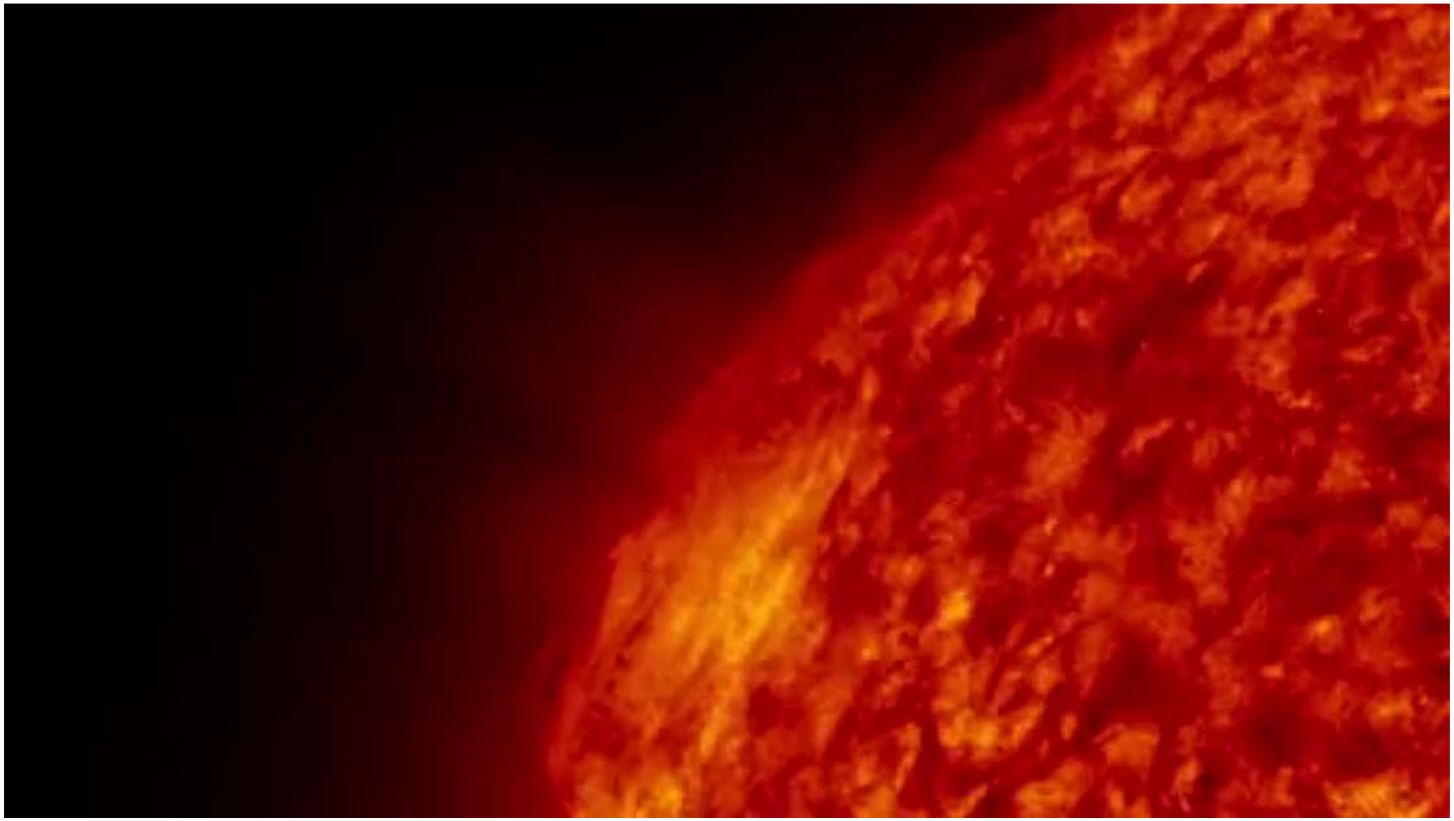

Courtesy: The Solar Dynamics Observatory

Magnetic reconnection layers in the magnetosphere

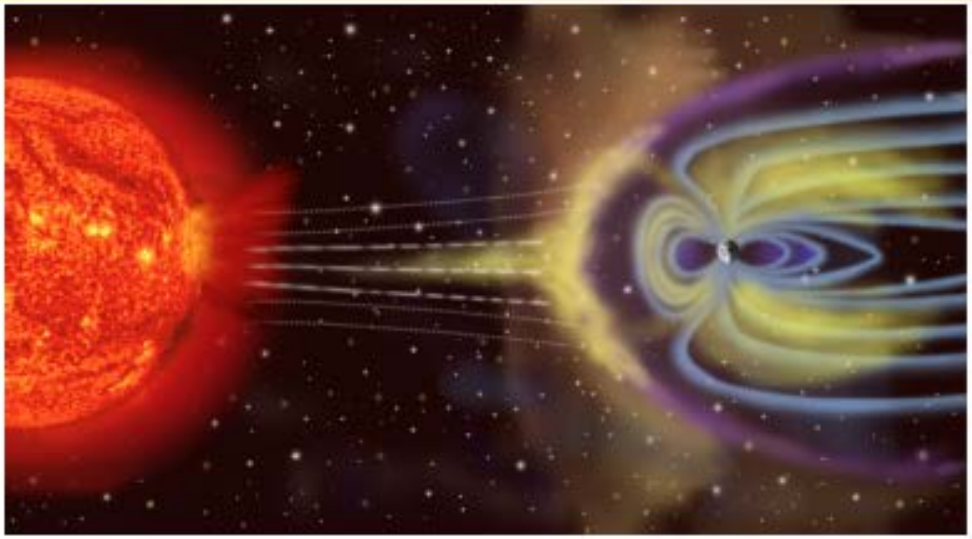

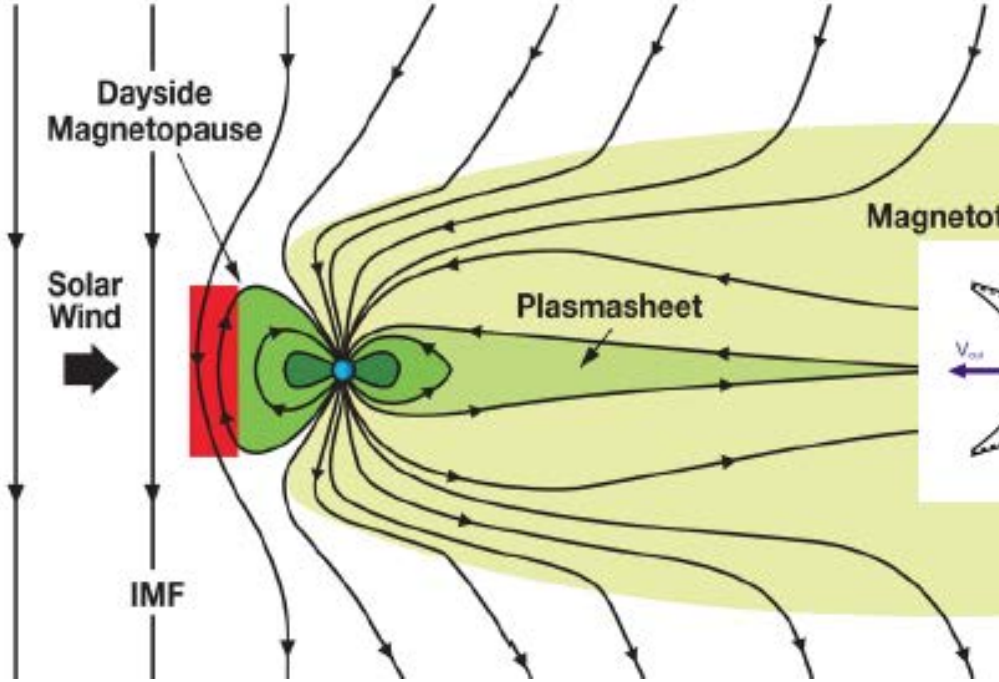

Data is available to evaluate inventory of energy flows

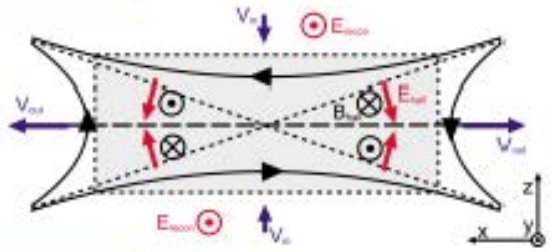

The Sweet-Parker Model for Magnetic Reconnection

Assume;

- 2D
- Steady-state
- Incompressibility
- Classical Spitzer resistivity

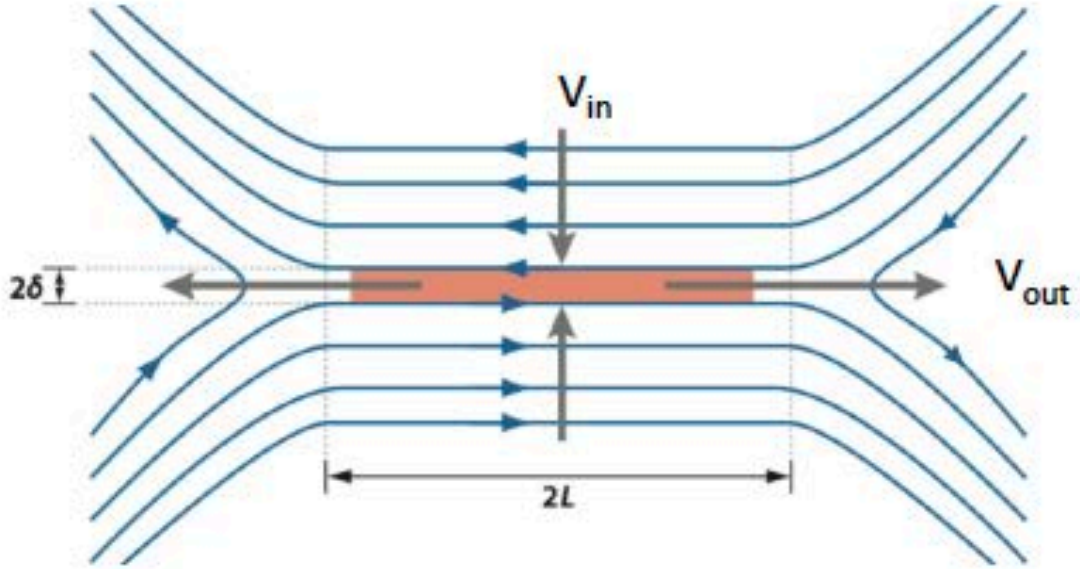

$$\frac{\partial \mathbf{B}}{\partial t} = \nabla \times (\mathbf{v} \times \mathbf{B}) + \frac{\eta}{\mu_0} \nabla^2 \mathbf{B} \quad \Rightarrow \quad V_{in} B = \frac{\eta_{Spitz}}{\mu_0} \frac{B}{\delta}$$

$$\frac{V_{in}}{V_A} = \frac{1}{\sqrt{S}}$$

Mass conservation: $V_{in} L \approx V_{out} \delta$

$$S = \frac{\mu_0 L V_A}{\eta_{Spitz}}$$

Pressure balance: $\frac{1}{2} \rho V_{out}^2 \approx \frac{B^2}{2\mu_0} \Rightarrow V_{out} \approx V_A$

S = Lundquist number

In solar flares, $\tau_{SP} \sim 1$ year $>> \tau_{reconn}$

Q. Why is Sweet-Parker reconnection so slow?

A. Geometry

Conservation relations of mass, energy, and flux

$$V_{in} L = V_{out} \delta, \quad V_{out} = V_A$$

$$V_{in} = \frac{\delta}{L} V_A, \quad \frac{\delta}{L} = S^{-1/2}$$

Petschek [1964]

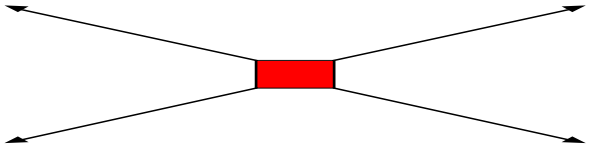

Geometry of reconnection layer: X-point

Length Δ ($<< L$) is of the order of the width δ

$$\tau_{PK} = \tau_A \ln S$$

Solar flares: $\tau_{PK} \sim 10^2 s$

Computational Tests of the Petschek Model

[Sato and Hayashi 1979, Ugai 1984, Biskamp 1986, Forbes and Priest 1987, Scholer 1989, Yan, Lee and Priest 1993, Ma et al. 1995, Uzdensky and Kulsrud 2000, Breslau and Jardin 2003, Malyshkin, Linde and Kulsrud 2005]

Conclusions

• Petschek model is not realizable in high-S plasmas, unless the resistivity is locally strongly enhanced at the X-point.
• In the absence of such anomalous enhancement, the reconnection layer evolves dynamically to form Y-points and realize a Sweet-Parker regime.

2D coronal loop : high-Lundquist number resistive MHD simulation

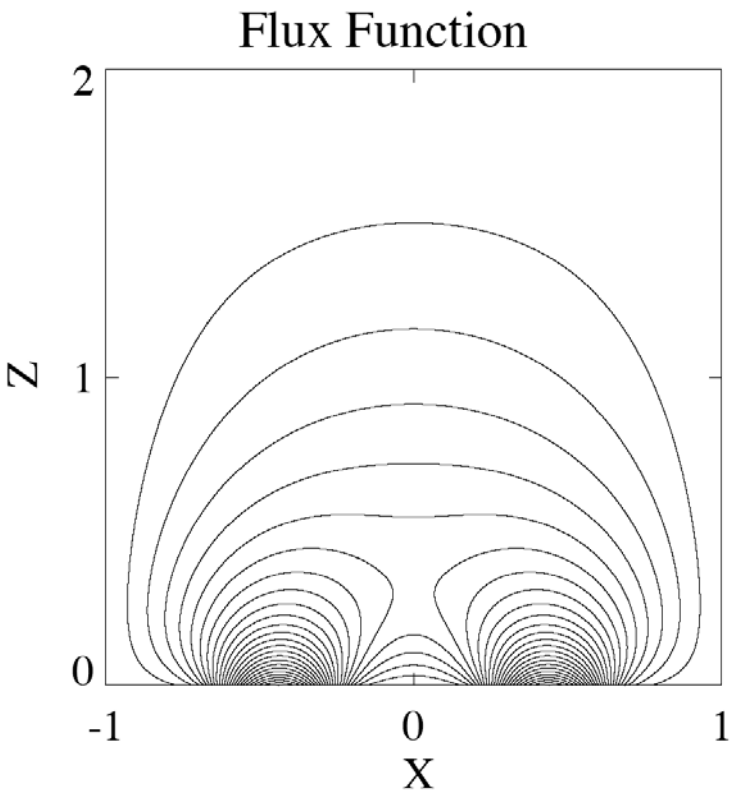

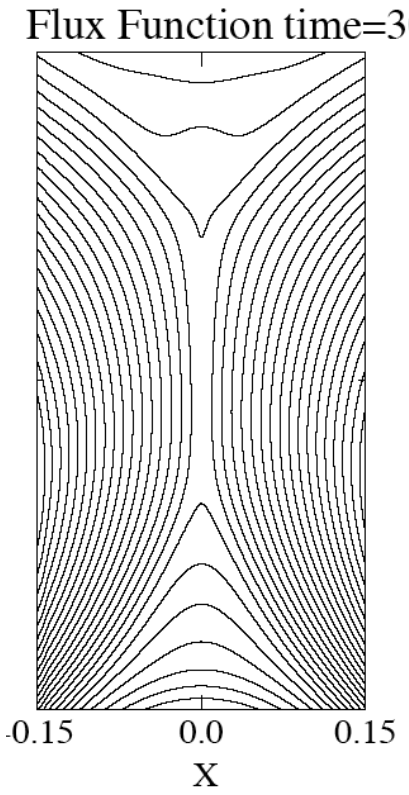

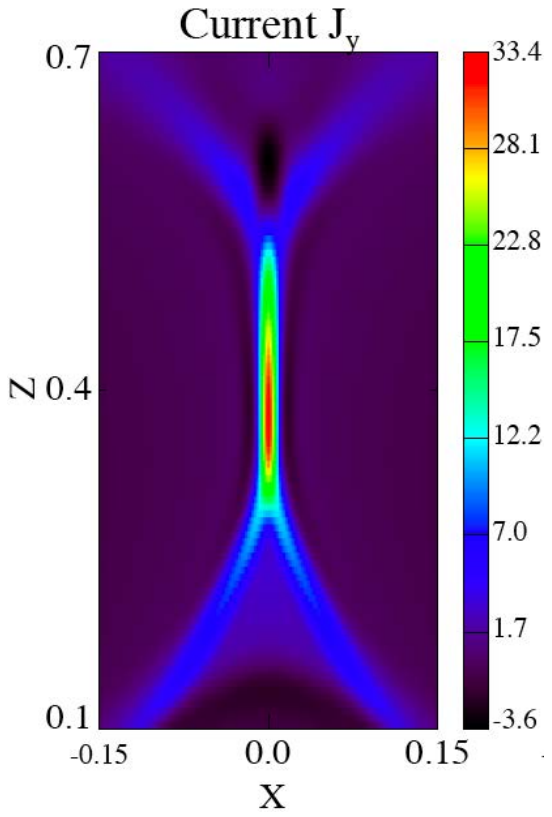

T = 0

T = 30

Impulsive Reconnection: The Onset/Trigger Problem

Dynamics exhibits an impulsiveness, that is, a sudden change in the time-derivative of the reconnection rate.

The magnetic configuration evolves slowly for a long period of time, only to undergo a sudden dynamical change over a much shorter period of time.
Dynamics is characterized by the formation of near-singular current sheets which need to be resolved in computer simulations: a classic multi-scale problem coupling large scales to small.

Examples

Magnetospheric substorms

Impulsive solar/stellar flares

Substorm Onset:
Where does it occur?

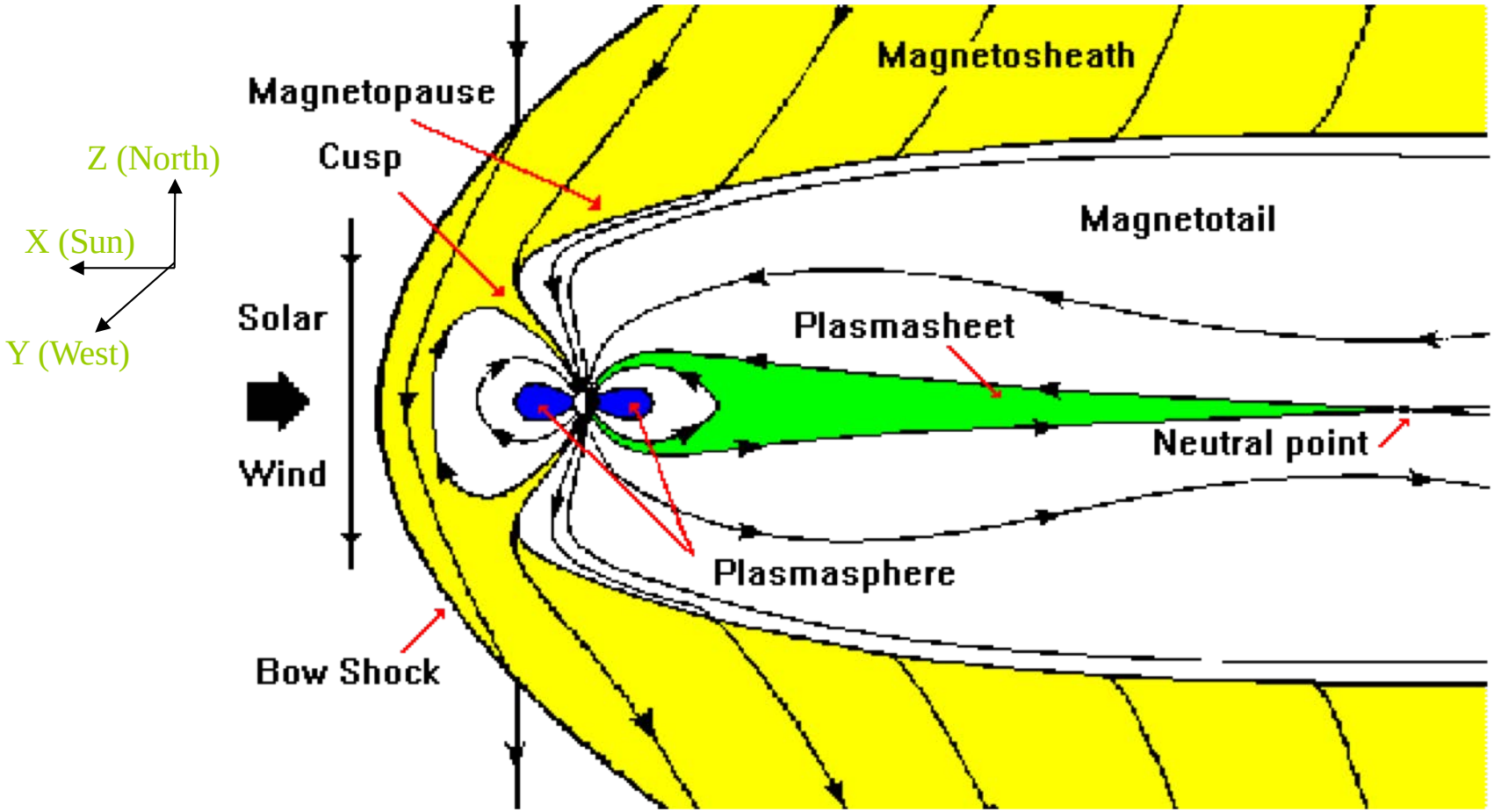

Substorm Onset:

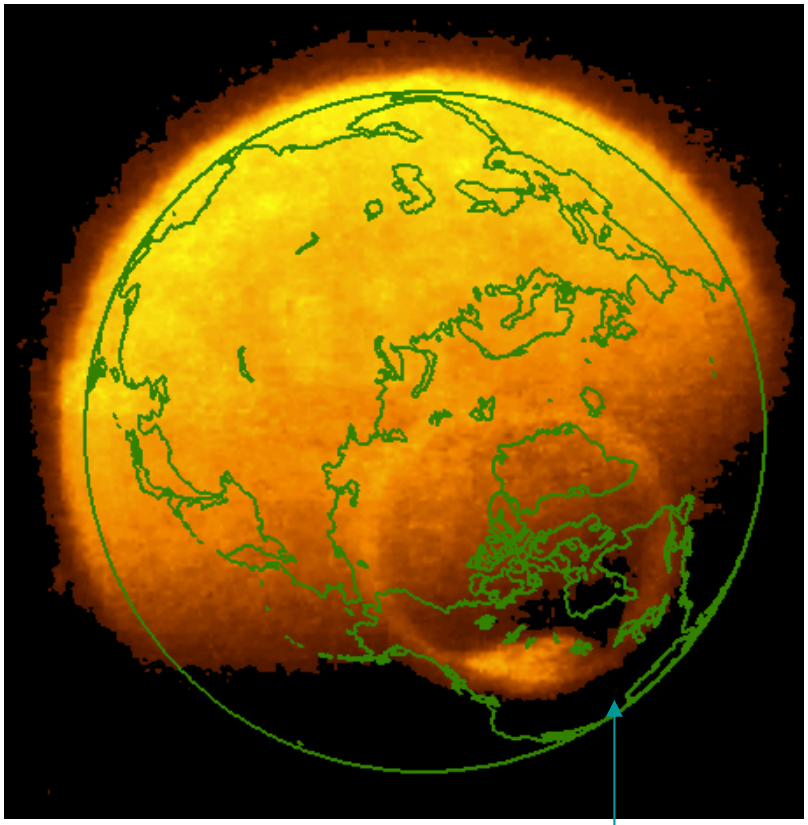

Auroral bulge

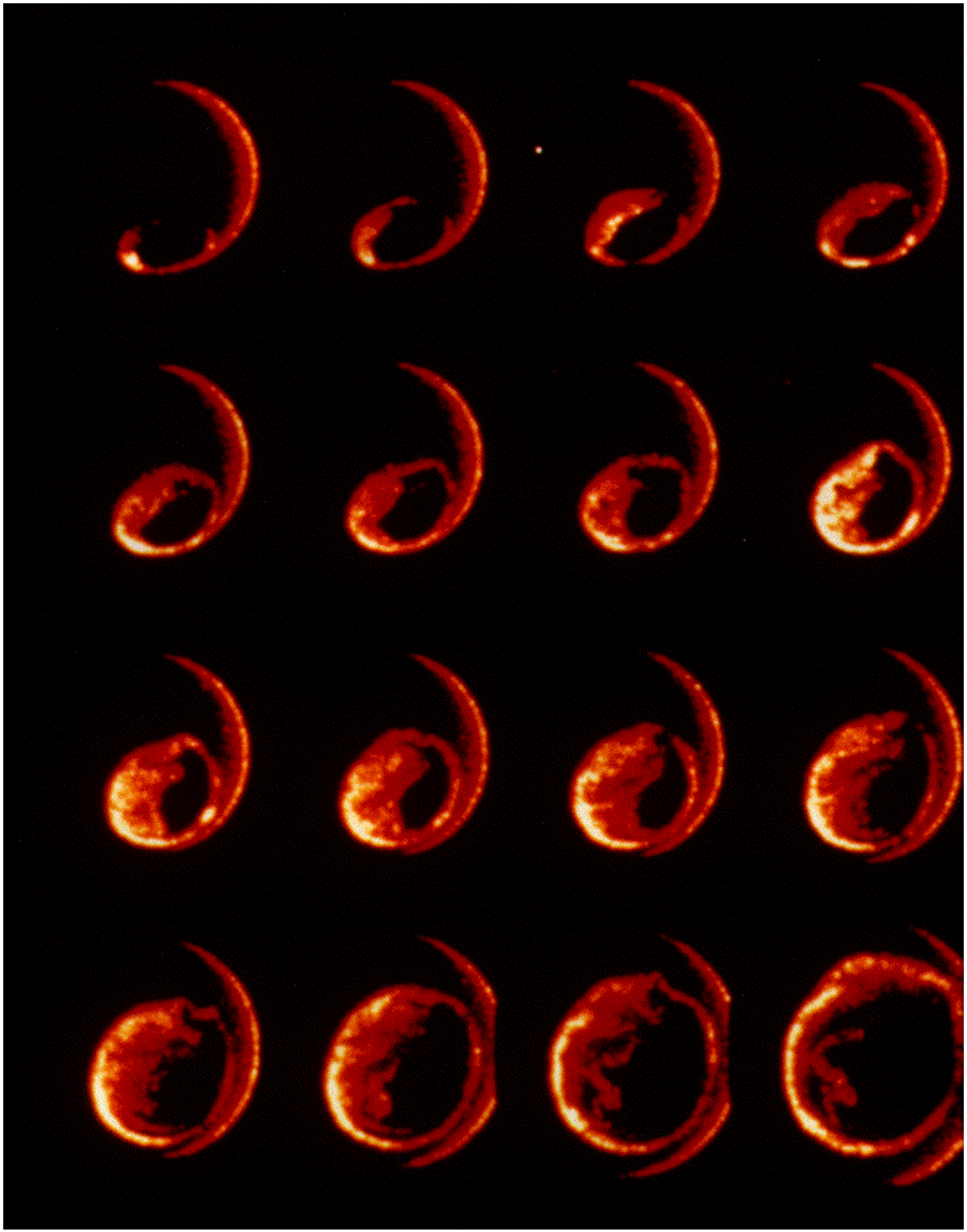

Substorm Onset: When does it occur?

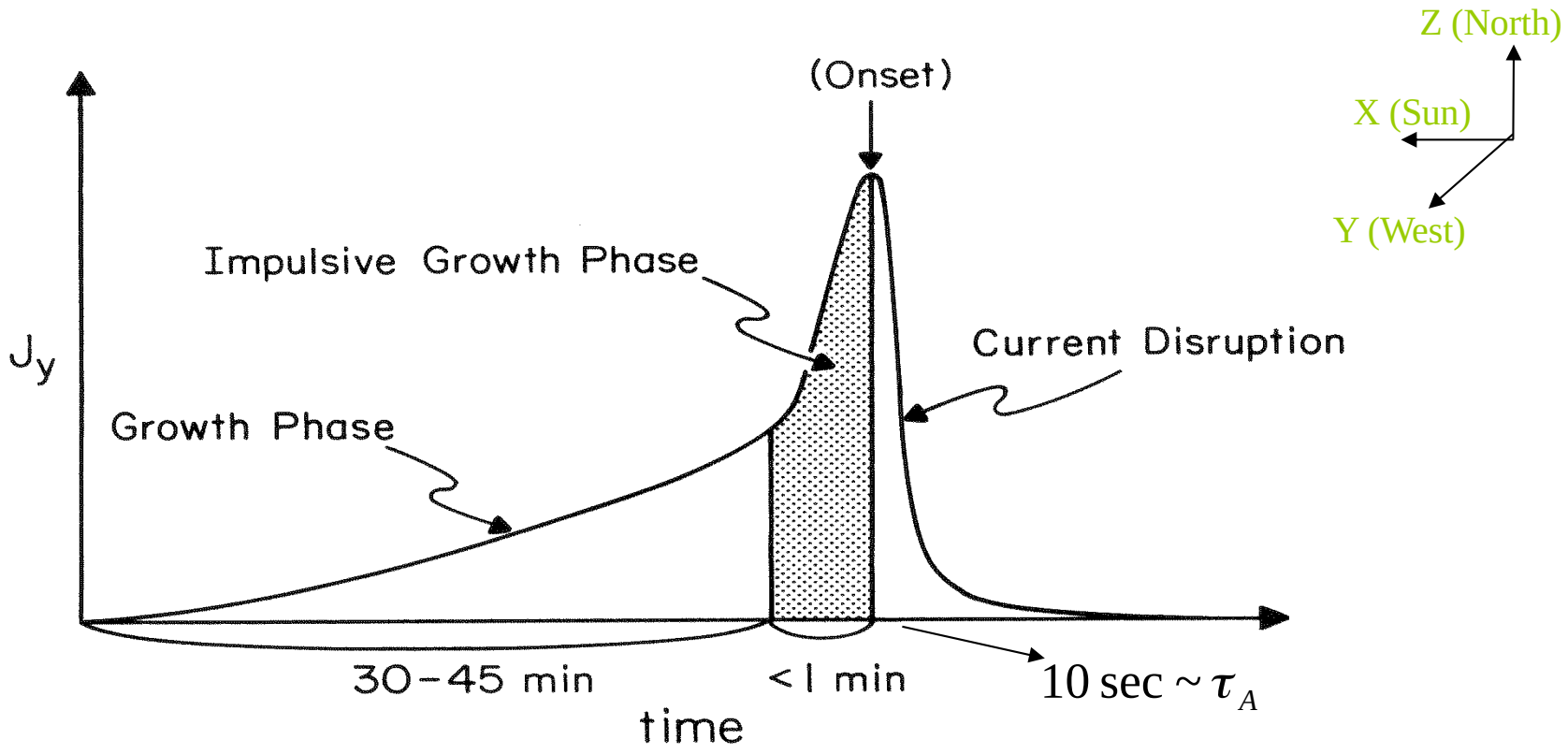

(Ohtani et al., 1992)

Growth Expansion Recovery

Generalized Ohm's law

What's really important?

$$\mathbf{E} = \underbrace{-\mathbf{v}_i \times \mathbf{B}}_{\text{(i)}} \underbrace{- \frac{m_e}{e}\frac{d\mathbf{v}_e}{dt}}_{\text{(ii)}} \underbrace{- \frac{1}{en_e}\nabla\cdot\vec{P}_e}_{\text{(iii)}} + \underbrace{\frac{1}{en_e}\mathbf{J}\times\mathbf{B}}_{\text{(iv)}} + \underbrace{\eta_e \mathbf{J}}_{\text{(v)}}$$

$$\frac{\text{(i)}}{\text{(v)}} = \frac{vB}{\eta_e B/\mu_0 \ell} = \frac{\ell v \mu_0}{\eta_e} \equiv R_m$$

$$\frac{\text{(i)}}{\text{(ii)}} = \frac{vB}{m_e vB/\mu_0 e^2 n_e \ell^2} = \frac{\ell^2}{m_e/\mu_0 e^2 n_e} = \left(\frac{\ell}{c/\omega_{pe}}\right)^2$$

$$\frac{\text{(i)}}{\text{(iv)}} = \frac{vB}{B^2/\mu_0 e n_e \ell} = \frac{v\ell}{B/\mu_0 e n_e} = \left(\frac{v}{v_A}\right)\left(\frac{\ell}{c/\omega_{pi}}\right)$$

$$\frac{\text{(i)}}{\text{(iii)}} = \frac{vB}{p_e/en_e\ell} = \frac{v\ell}{k_B T/eB} = \left(\frac{v}{c_s}\right)\left(\frac{\ell}{\rho_i}\right)$$

Importance of term depends on length scale of solution

On large scales plasma is ideal conductor*

* except where **B**=0

Hall MHD (or Extended MHD) Model and the Generalized Ohm's Law

In high-*S* plasmas, when the width of the thin current sheet (Δ_η) satisfies

$$\Delta_\eta < c/\omega_{pi} \qquad \text{(or } \rho_s \equiv \sqrt{\beta} c/\omega_{pi} \text{ if there is a guide field)}$$

"collisionless" terms in the generalized Ohm's law cannot be ignored.

Generalized Ohm's law (dimensionless form)

$$\mathbf{E} + \mathbf{v} \times \mathbf{B} = \frac{1}{S}\mathbf{J} + d_e^2 \frac{d\mathbf{J}}{dt} + \frac{d_i}{n}\left(\mathbf{J} \times \mathbf{B} - \nabla p_e\right)$$

Electron skin depth $\quad d_e \equiv L^{-1}\left(c/\omega_{pe}\right)$

Ion skin depth $\quad d_i \equiv L^{-1}\left(c/\omega_{pi}\right)$

Electron beta $\quad \beta_e$

Forced Magnetic Reconnection Due to Inward Boundary Flows

Magnetic field

$$\mathbf{B} = \hat{\mathbf{x}} B_P \tanh z/a + \hat{\mathbf{z}} B_T$$

Inward flows at the boundaries

$$\mathbf{v} = \mp V_0 (1 + \cos kx)\hat{\mathbf{y}} \qquad , \qquad \Delta' < 0$$

Two simulations: Resistive MHD versus Hall MHD [Ma and B. 1996]

For other perspectives, with similar conclusions, see Grasso et al. (1999) Dorelli and Birn (2003), Fitzpatrick (2004), Cassak et al. (2005), Simakov and Chacon (2008), Malyshkin (2008)

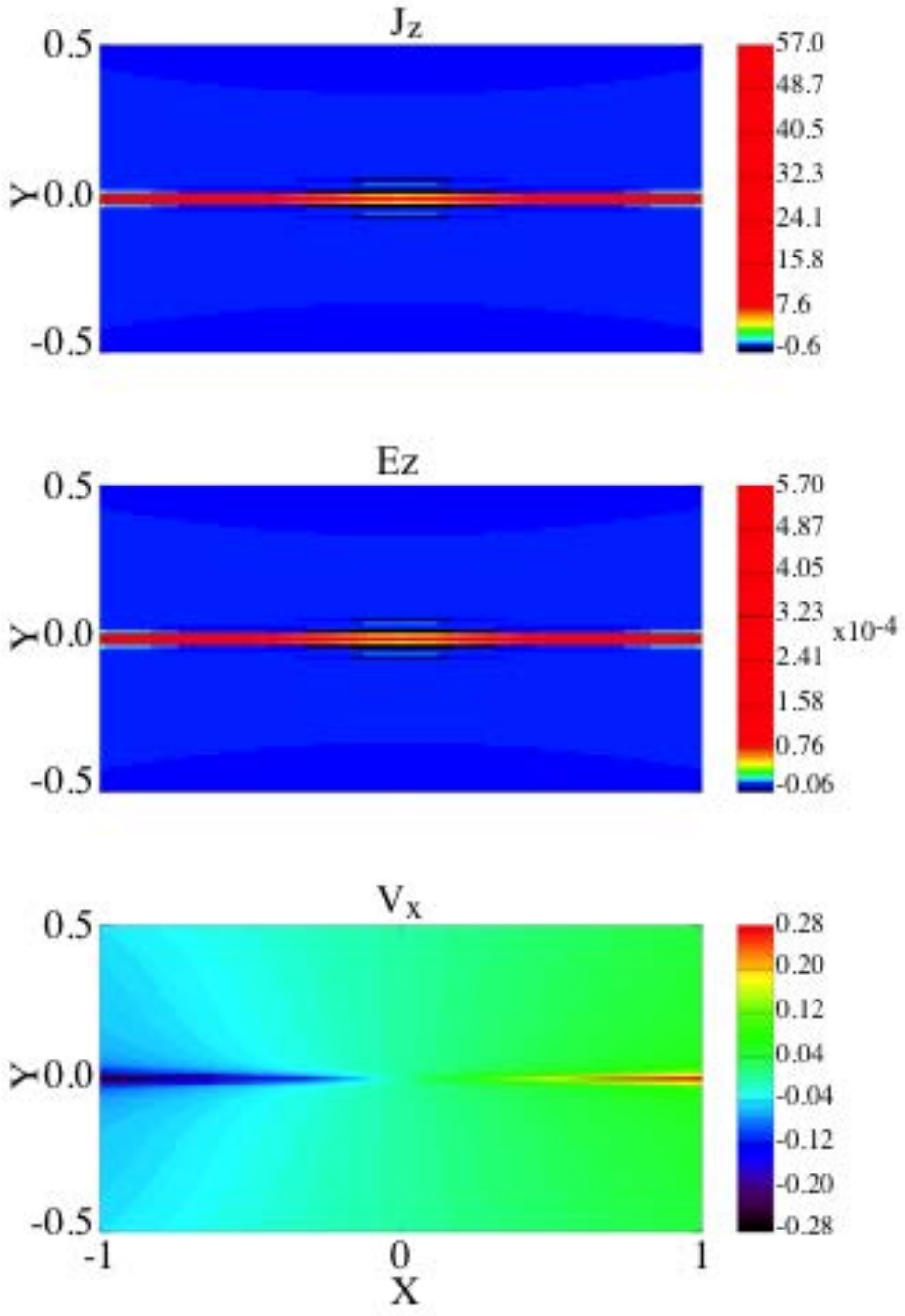
Jz
0.5
Y 0.0
-0.5
57.0
48.7
40.5
32.3
24.1
15.8
7.6
-0.6
Ez
0.5
Y 0.0
-0.5
5.70
4.87
4.05
3.23
2.41
1.58
0.76
-0.06
x10-4
Vx
0.5
Y 0.0
-0.5
-1
0
1
X
0.28
0.20
0.12
0.04
-0.04
-0.12
-0.20
-0.28

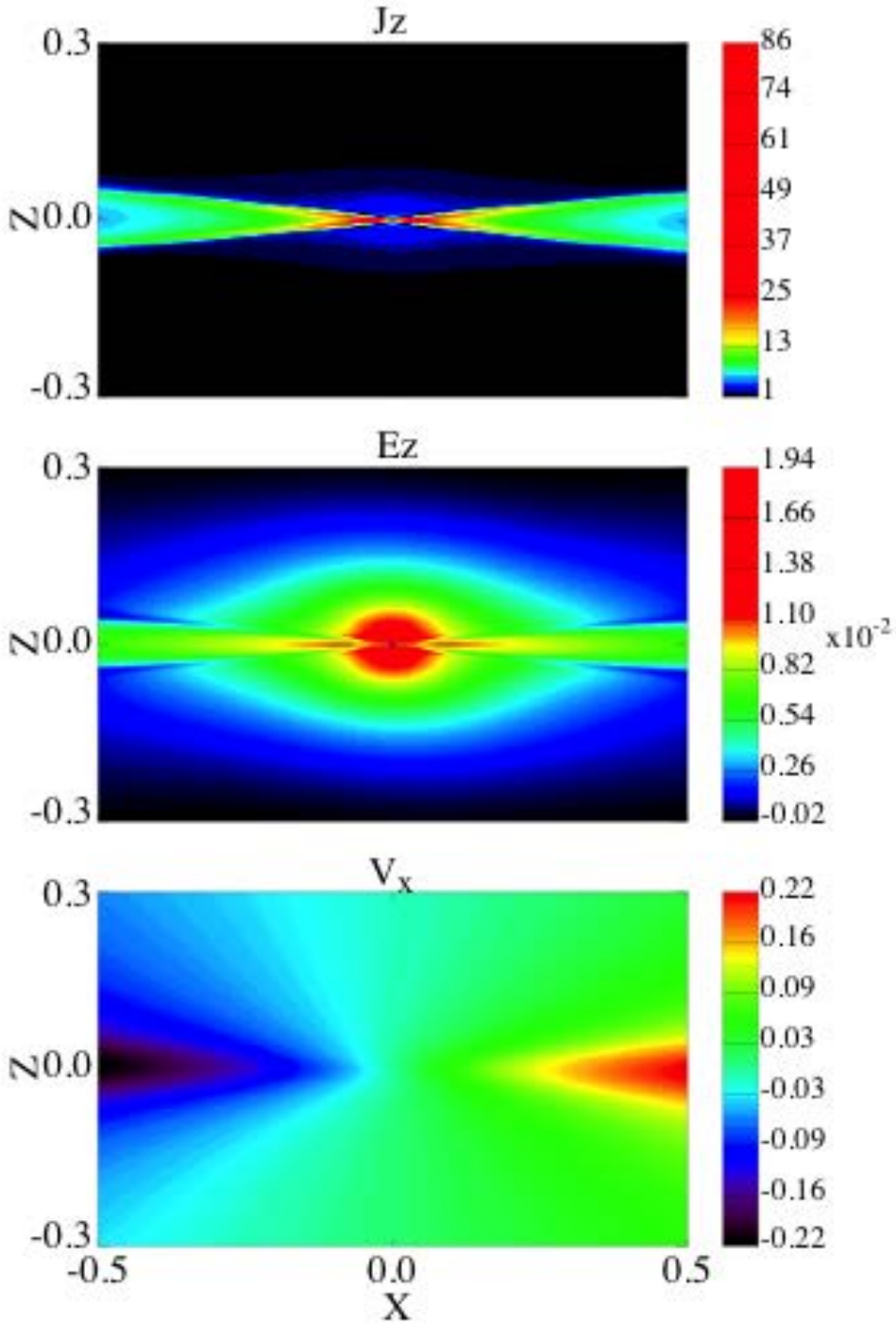
Jz
0.3
Z0.0
-0.3
86
74
61
49
37
25
13
1
Ez
0.3
Z0.0
-0.3
1.94
1.66
1.38
1.10
0.82
0.54
0.26
-0.02
x10-2
Vx
0.3
Z0.0
-0.3
0.22
0.16
0.09
0.03
-0.03
-0.09
-0.16
-0.22
-0.5
0.0
0.5
X

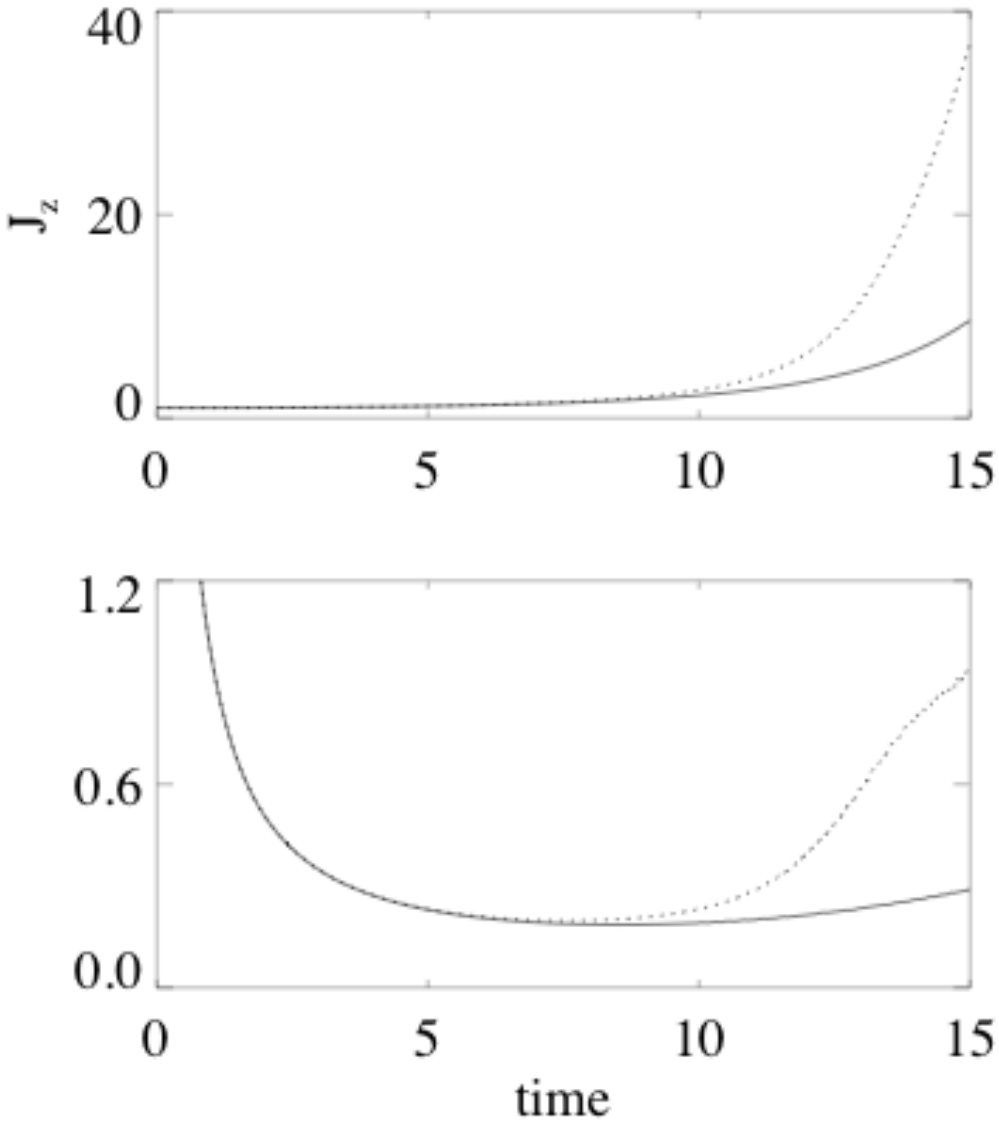

….. Hall

___ Resistive

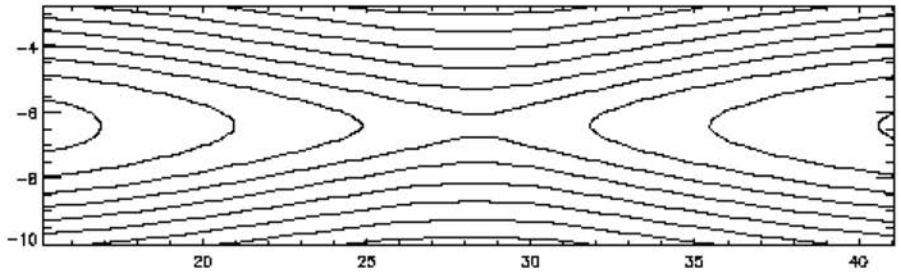

Field lines

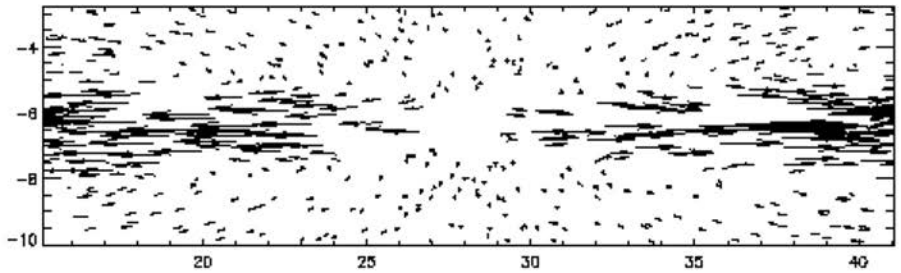

Electron flows

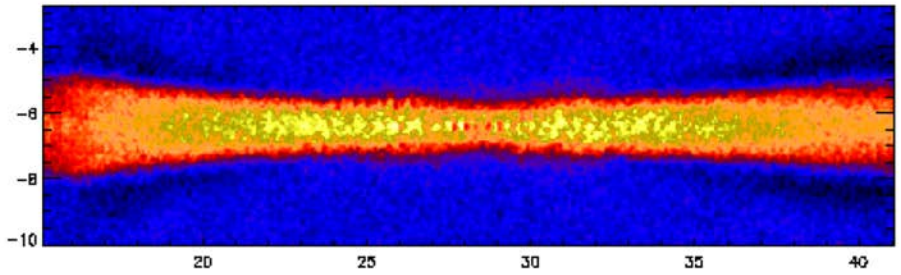

Ion current density

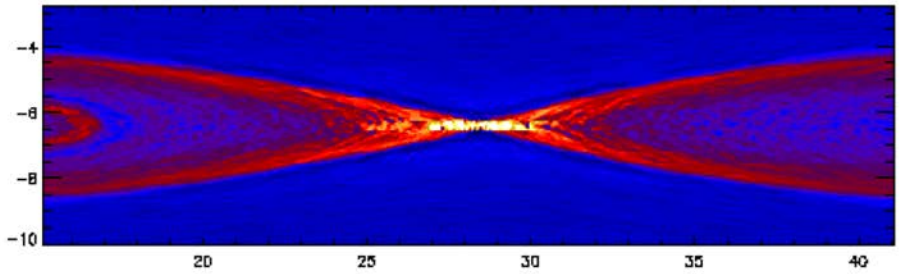

Electron current density

Transition from Collisional to Collisionless Regimes in MRX

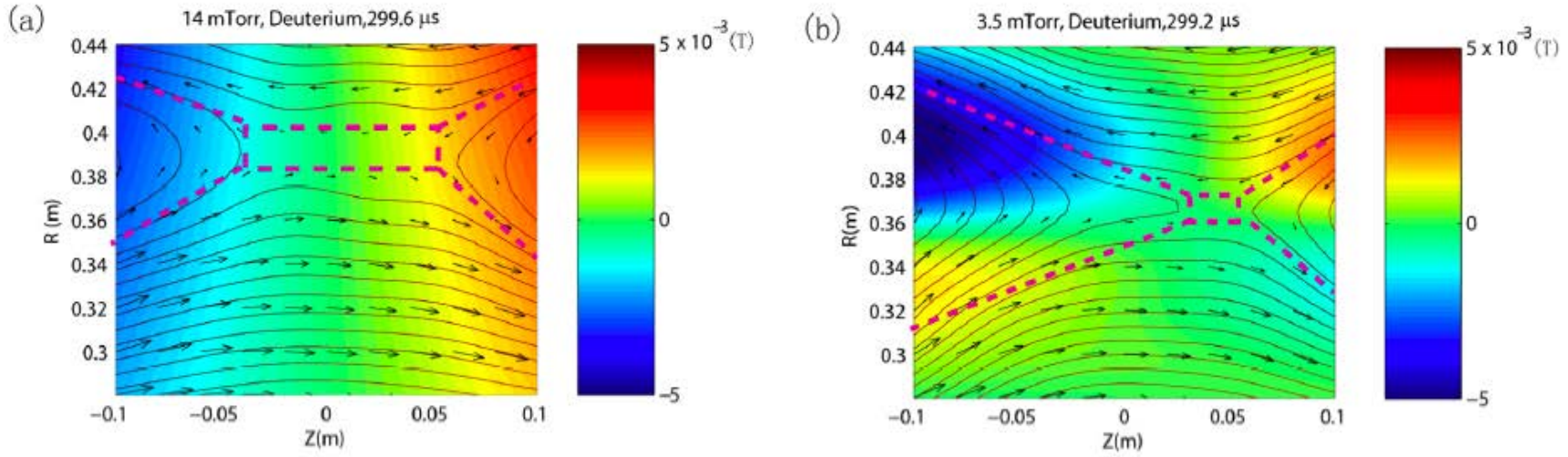

***Fig.2**; Comparison of neutral sheet configuration described by measured magnetic field vectors and flux counters for high (collisional) and low density cases; (a) Collisional regime (λ_{mfp} ~1mm << δ)); (b) Nearly collisionless regime (λ_{mfp} ~1cm ~ δ). Out-of plane fields are depicted by the color codes ranged -50 G <Bt <50 G.*

Linkage between space and laboratory plasmas

System	L (cm)	B (G)	$d_i = c/\omega_{pi}$(cm)	δ_{sp} (cm)	d_i/δ_{sp}
MRX	10	100-500	1-5	0.1-5	.2-100
Tokamak	100	10^4	10	0.1	100
Magnetosphere	10^9	10^{-3}	10^7	10^4	1000
Solar flare	10^9	100	10^4	10^2	100
ISM	10^{18}	10^{-6}	10^7	10^{10}	0.001
Proto-star		$d_i/\delta_s >> 1$			

$$d_i/\delta_{sp} \sim 5(\lambda_{mfp}/L)^{1/2}$$

PPPL PRINCETON PLASMA PHYSICS LABORATORY

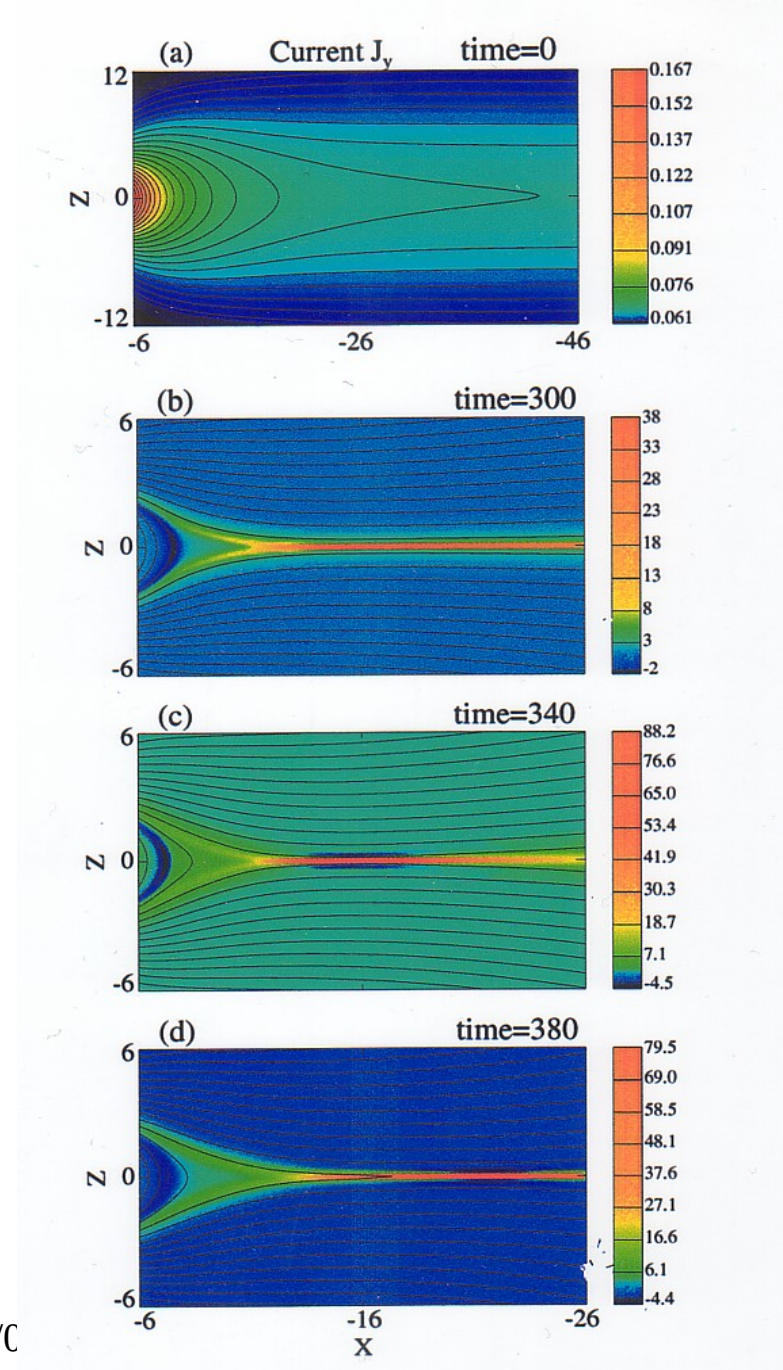

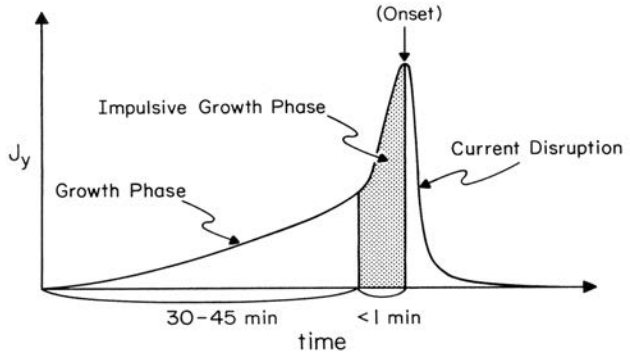

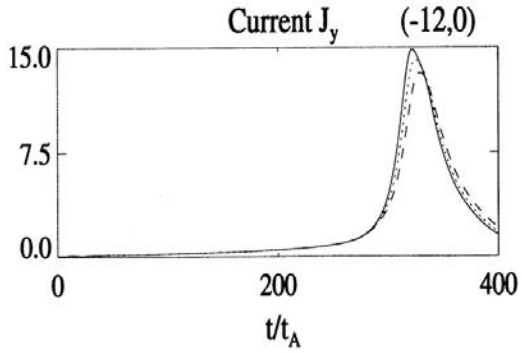

2D Hall-MHD Simulation

(Ma and B., 1998)

Plasmoid Instability of *Large-Scale* Current Sheets

Sweet-Parker (Sweet 1958, Parker 1957)

Geometry of reconnection layer : Y-points (Syrovatsky 1971)

Length of the reconnection layer is of the order of the system size >> width Δ

Reconnection time scale

$$\tau_{SP} = \left(\tau_A \tau_R\right)^{1/2} = S^{1/2}\tau_A$$

Solar flares: $S \sim 10^{12}, \quad \tau_A \sim 1s$

$$\Rightarrow \tau_{SP} \sim 10^6 s$$ Too long!

Fast Reconnection in Large Systems

- Extended thin current sheets of high Lundquist number are unstable to a super-Alfvenic tearing instability (Loureiro et al. 2007), which we call the "plasmoid instability," because it generates a large number of plasmoids.
- In the nonlinear regime, the reconnection rate becomes nearly independent of the Lundquist number, and is much larger than the Sweet-Parker rate.

The thin current sheet is explosively stable if we exceed a critical Lundquist number, S_c forming, ejecting, and coalescing a hierarchy of plasmoids.

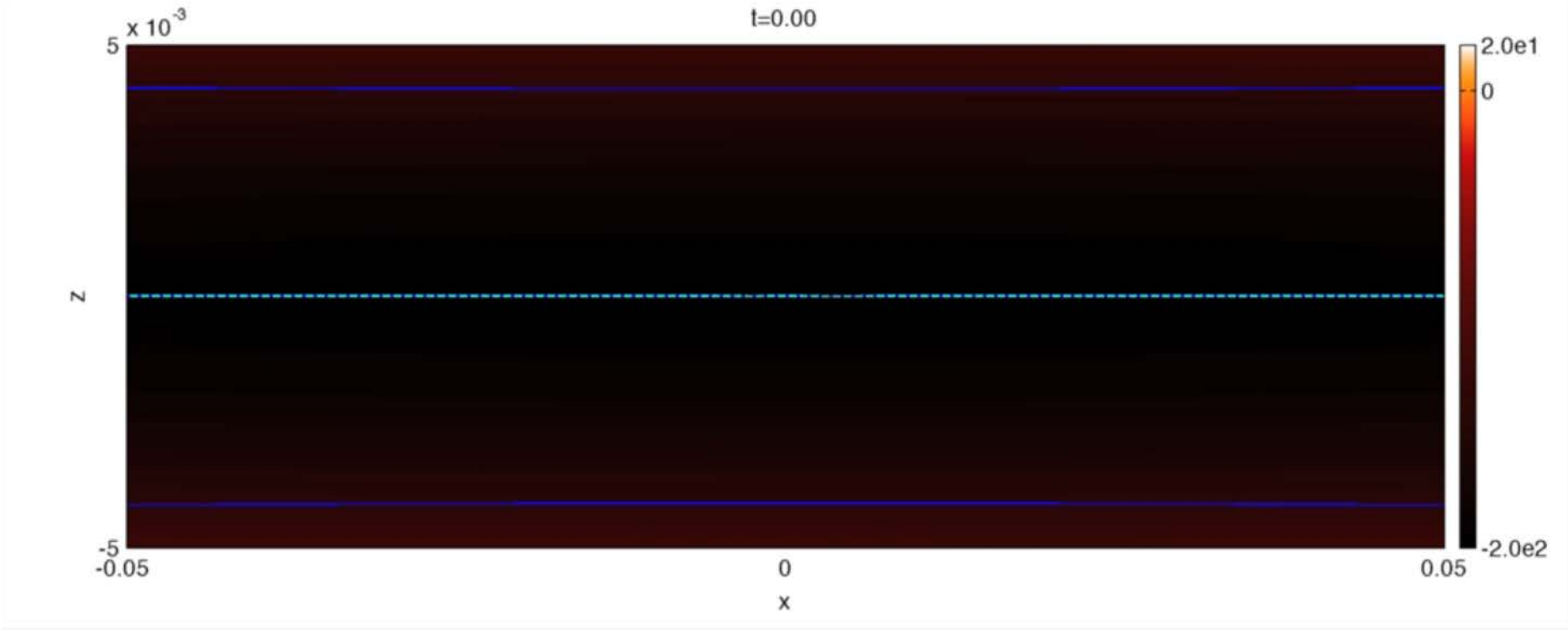

B. et al. 2009, Huang and B. 2010, Uzdensky et al. 2010

A little history

- Secondary tearing instability of high-S current sheet has been known for some time (Bulanov et al. 1979, Lee and Fu 1986, Biskamp 1986, Matthaeus and Lamkin 1986, Yan et al. 1992, Shibata and Tanuma 2001), but its precise scaling properties were determined only recently.
- The instability has been studied recently nonlinearly in fluid (Lapenta 2008, Cassak et al. 2009; Samtaney et al. 2009) as well as fully kinetic studies with a collision operator (Daughton et al. 2009).

Reconnection Time of 25% of Initial Flux

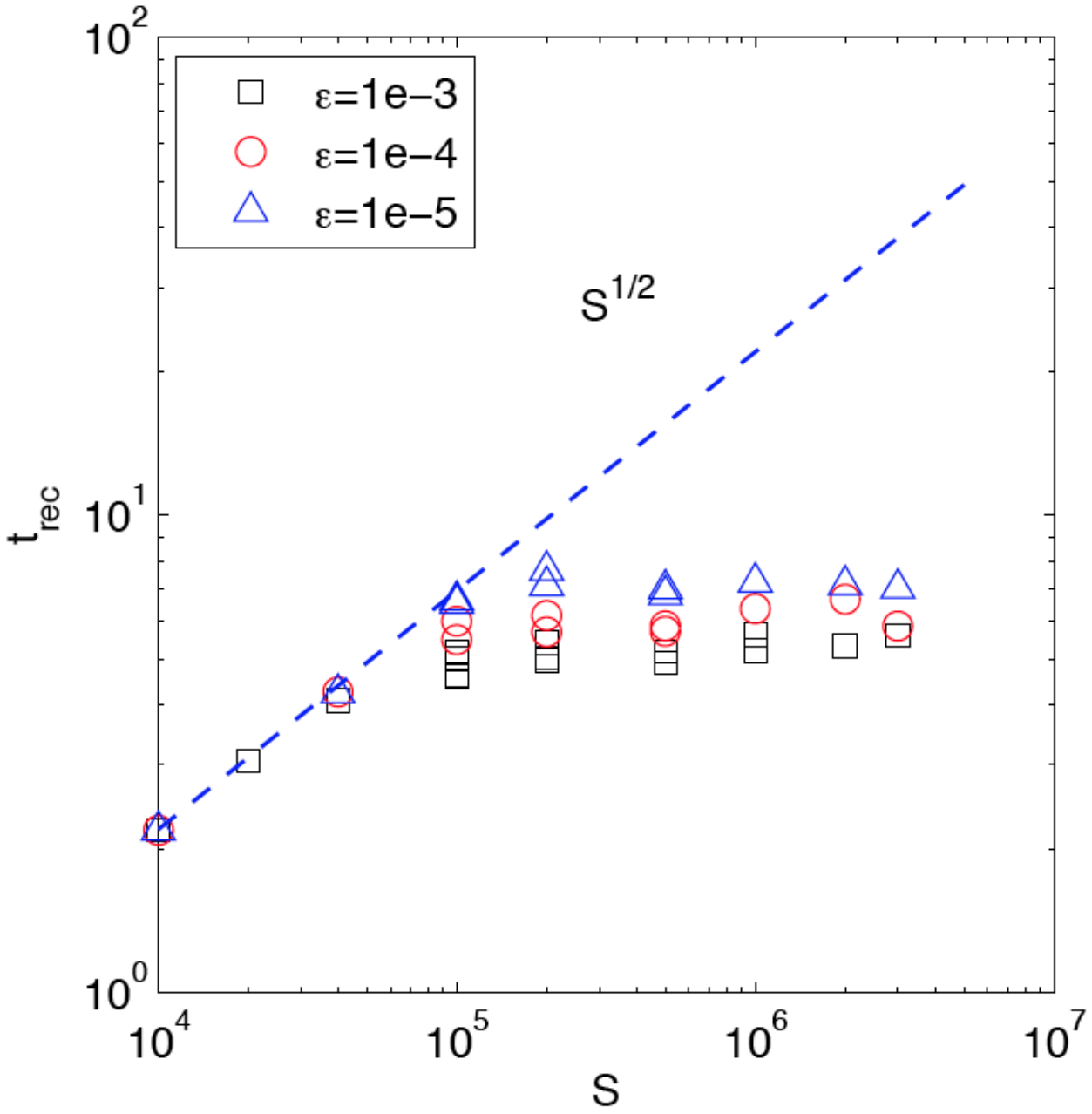

$$< \frac{1}{V_A B} \frac{d\psi}{dt} > \sim 0.01$$

$$< u_i > \sim 0.01 V_A$$

Heuristic Scaling Argument Based on Marginal Stability

- Cascade to smaller scales will stop when local current sheets become stable to the plasmoid instability
- New plasmoids are generated when local current sheets exceed a critical length.
- Consider the reconnection layer as a chain of plasmoids connected by marginally stable current sheets. For a critical Lundquist number S_c:
  - Critical length $L_c \sim S_c \eta / V_A \sim L S_c / S$
  - Number of plasmoids $n_p \sim L / L_c \sim S / S_c$
  - Current sheet with $\delta_c \sim L_c / S_c^{1/2} \sim L S_c^{1/2} / S$
  - Current density $J \sim B / \delta_c \sim B S / L S_c^{1/2}$
  - Reconnection rate $\sim \eta J \sim \eta B / \delta_c \sim B V_A / S_c^{1/2}$, which is independent of S

Parameter Space

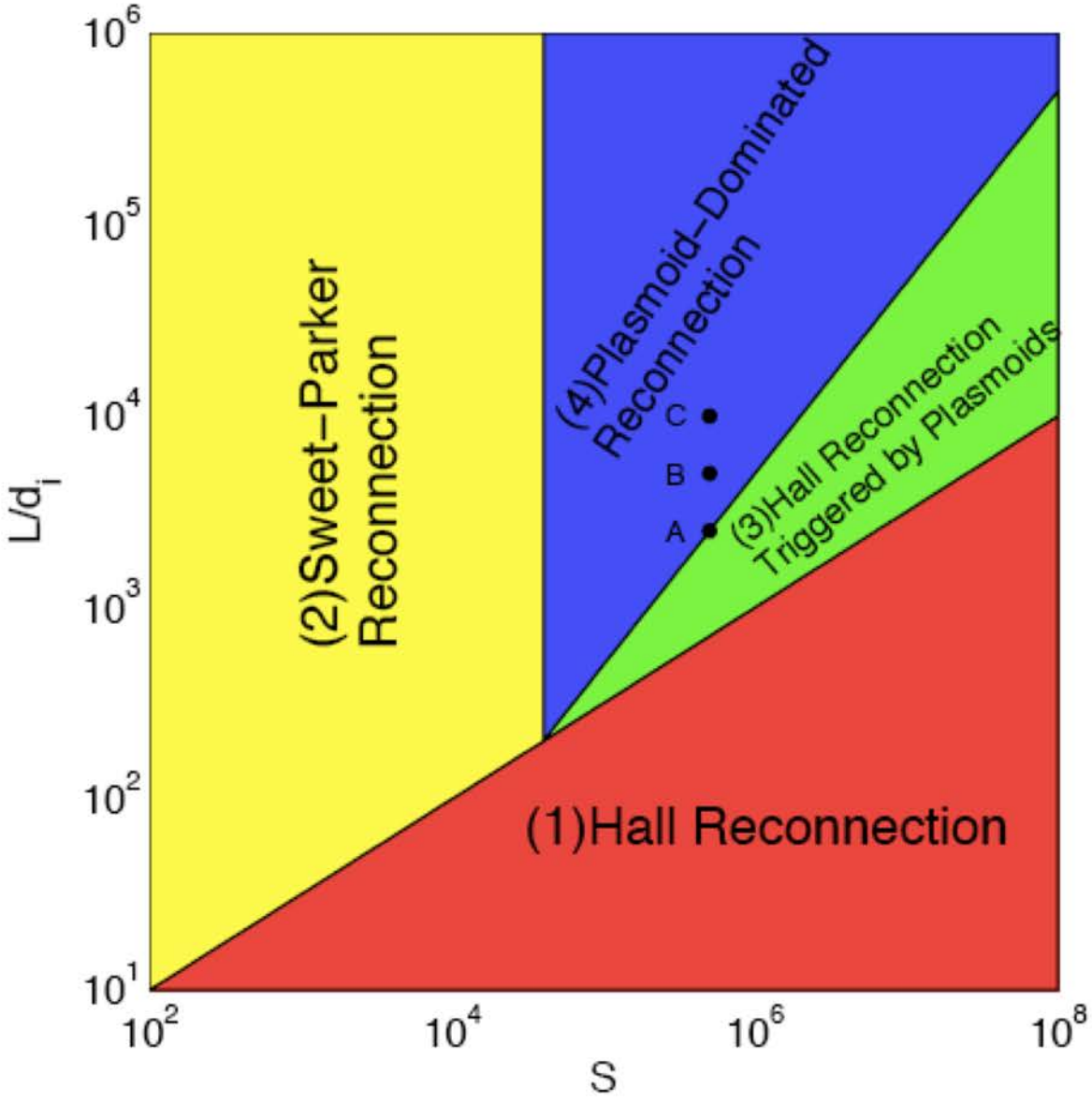

A: $S = 5 \times 10^5, d_i = 4 \times 10^{-4}$
B: $S = 5 \times 10^5, d_i = 2 \times 10^{-4}$
C: $S = 5 \times 10^5, d_i = 10^{-4}$
D: $S = 5 \times 10^5, d_i = 0$

Reconnection Rate

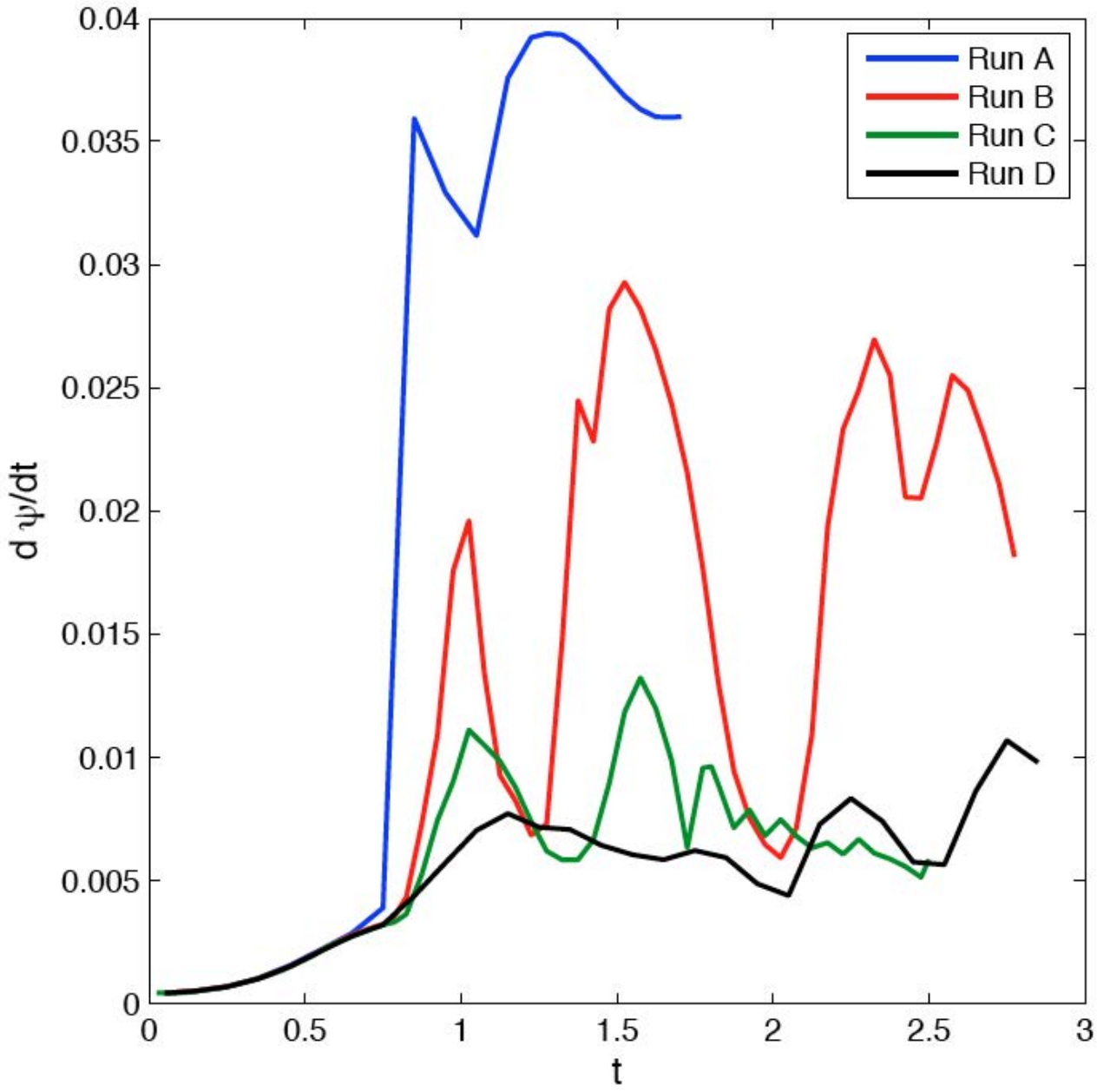

Run A, global configuration at late time

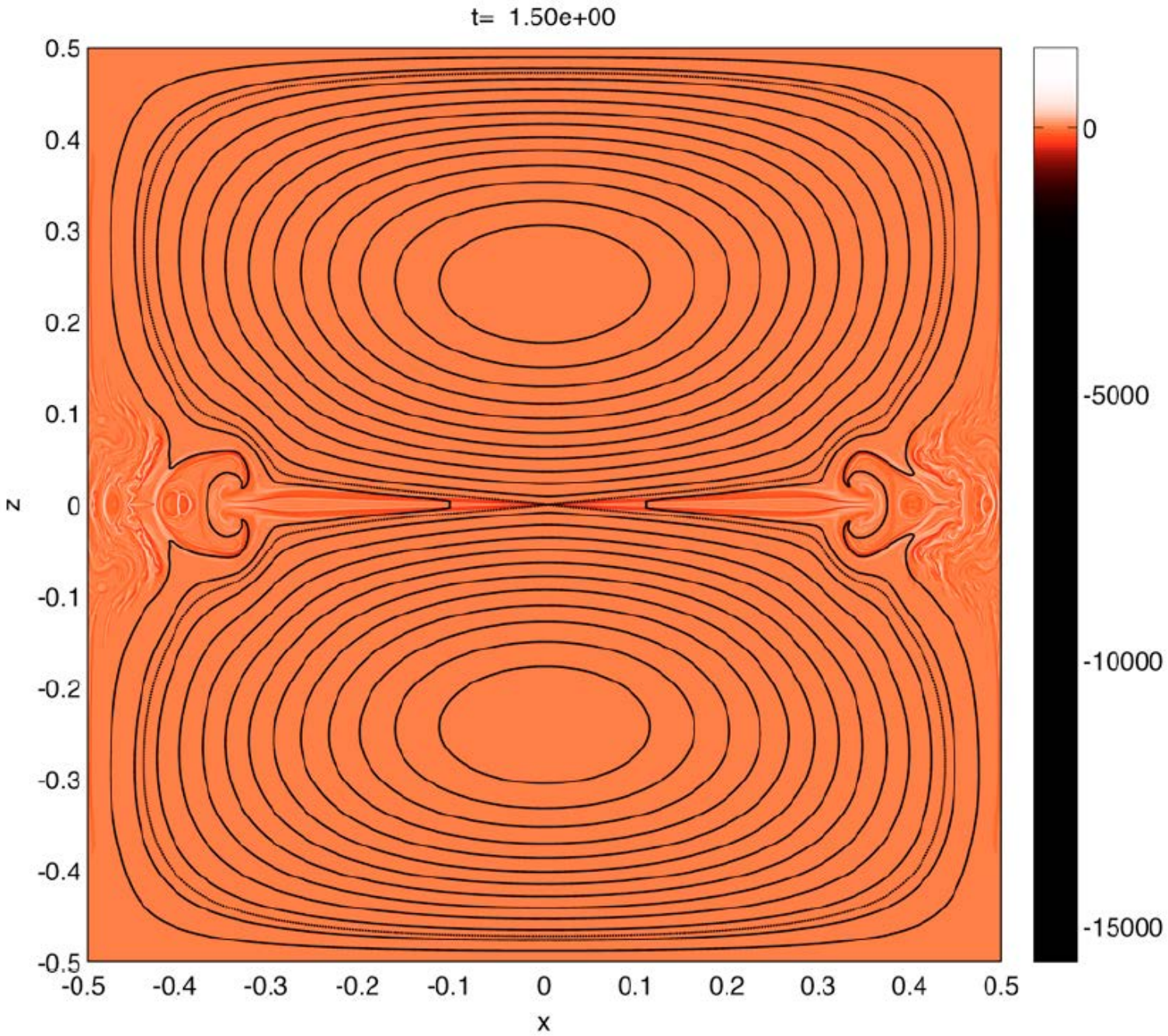

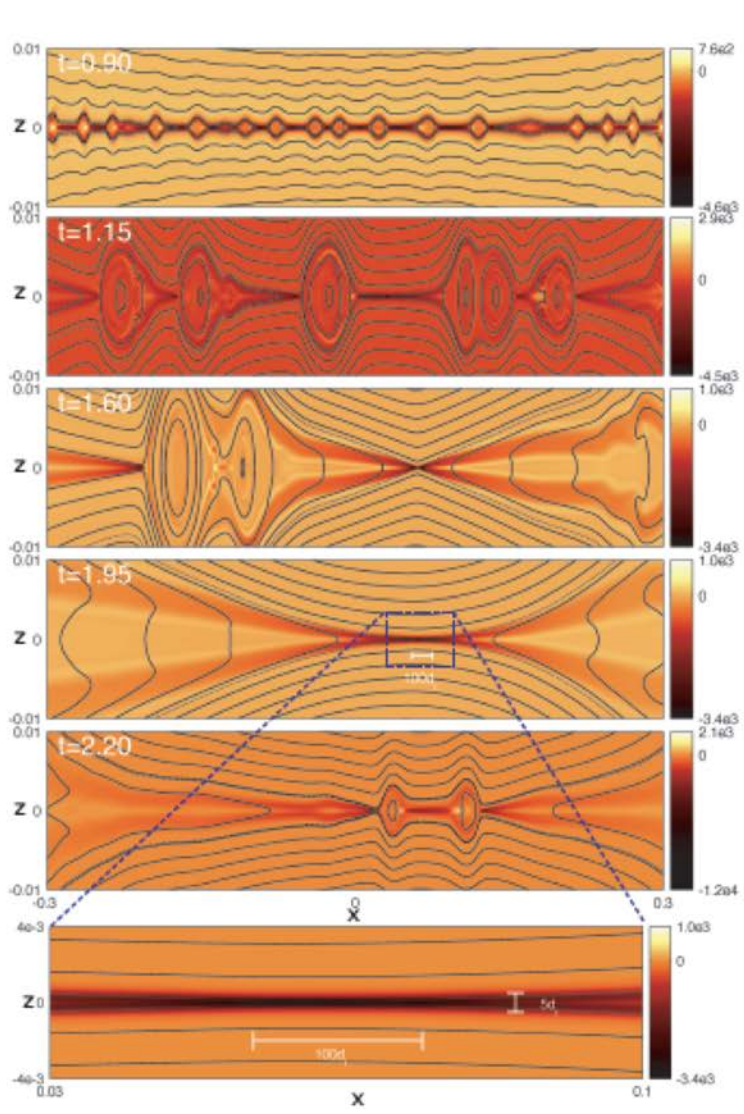

Run B, resistive Hall

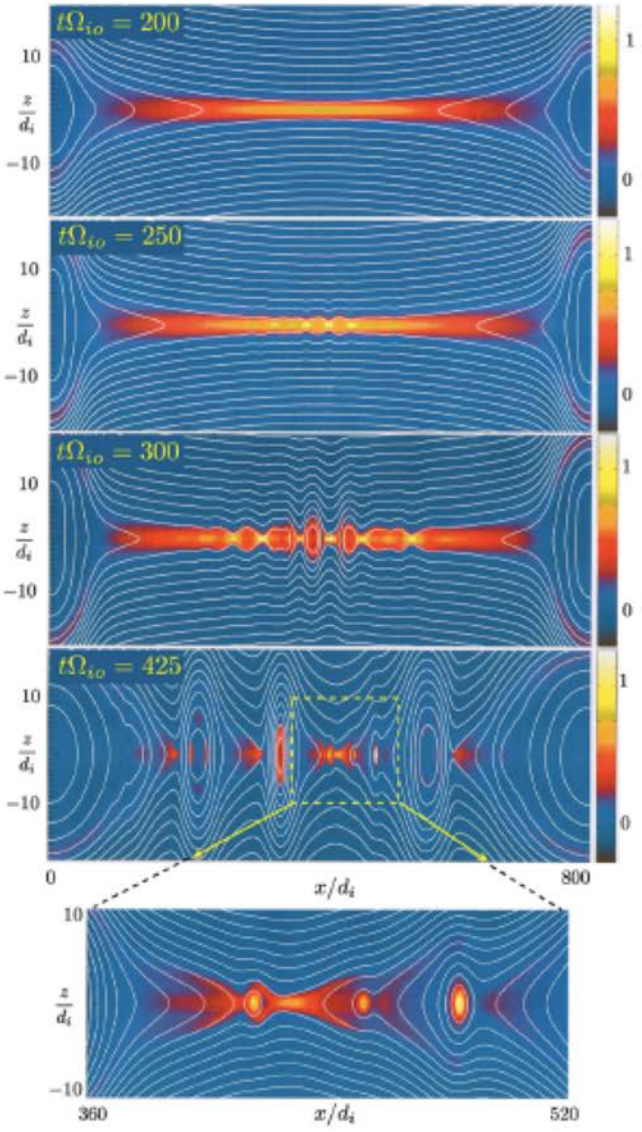

Daughton et al. (2009), PIC

Largest 2D Hall MHD simulation to date

Observations of energetic electrons within magnetic islands

[Chen et al., Nature Phys., 2008, PoP 2009]

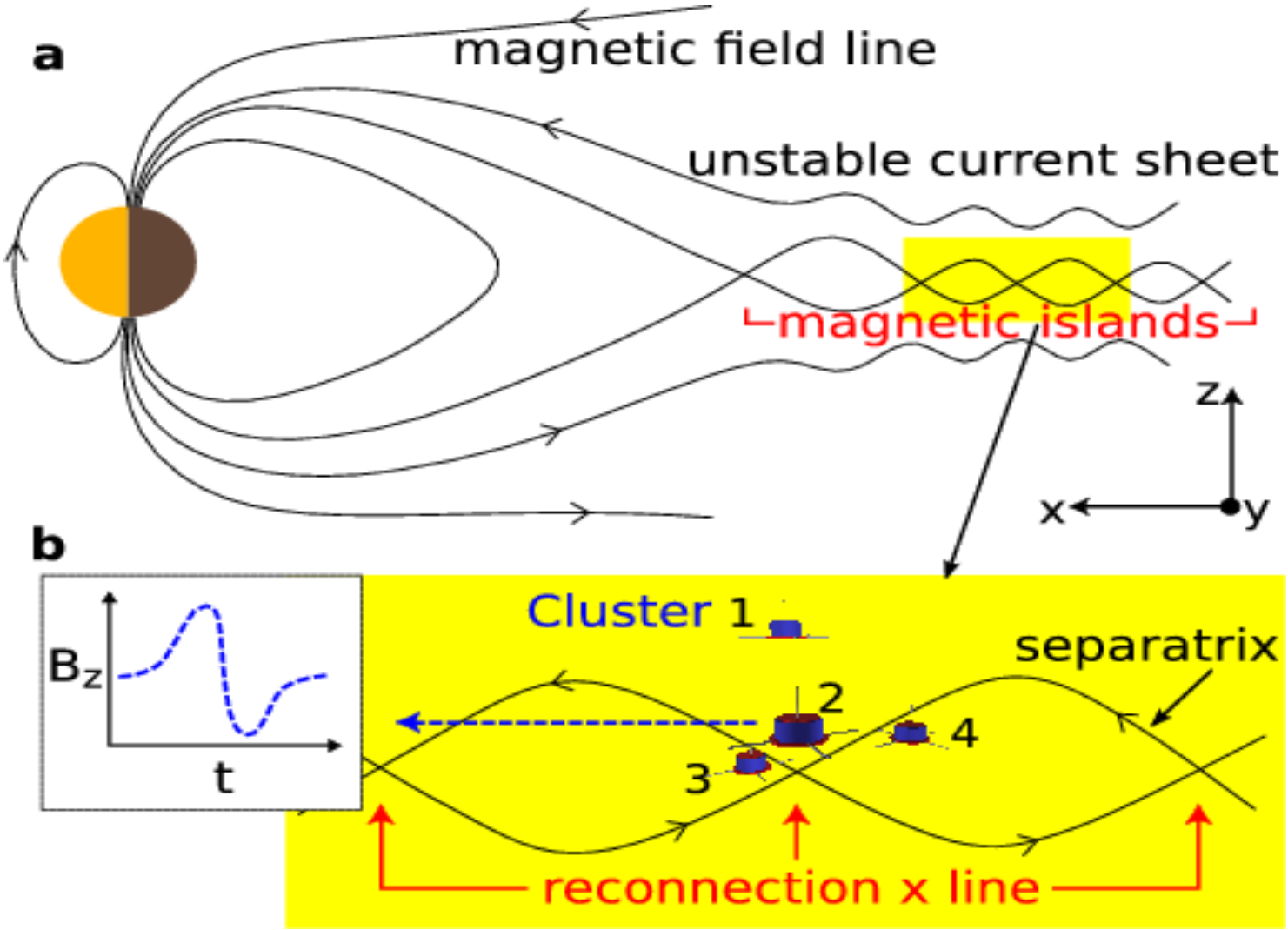

e bursts & bipolar Bz & Ne peaks

~10 islands within 10 minutes

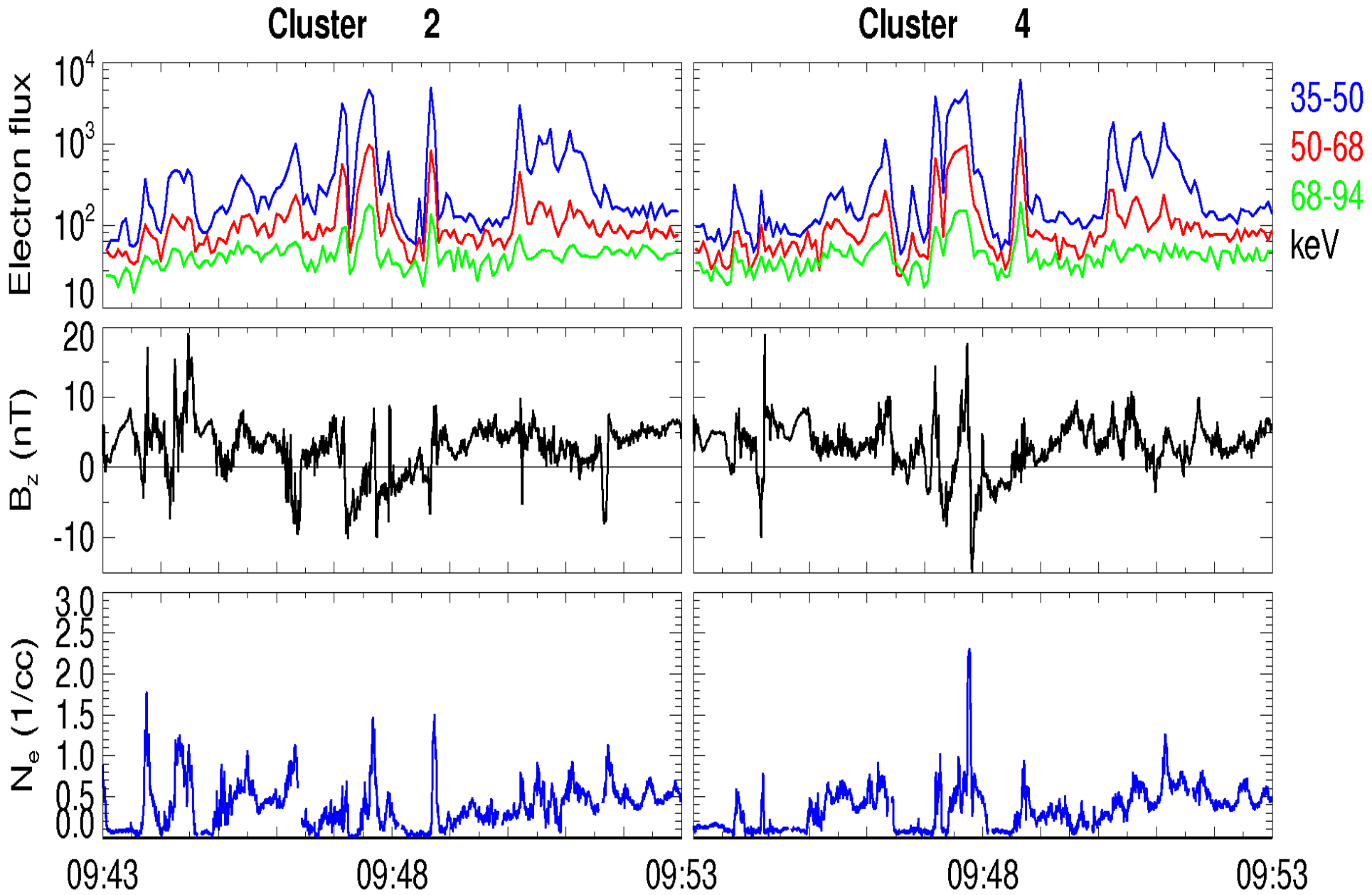

Post CME Current Sheet

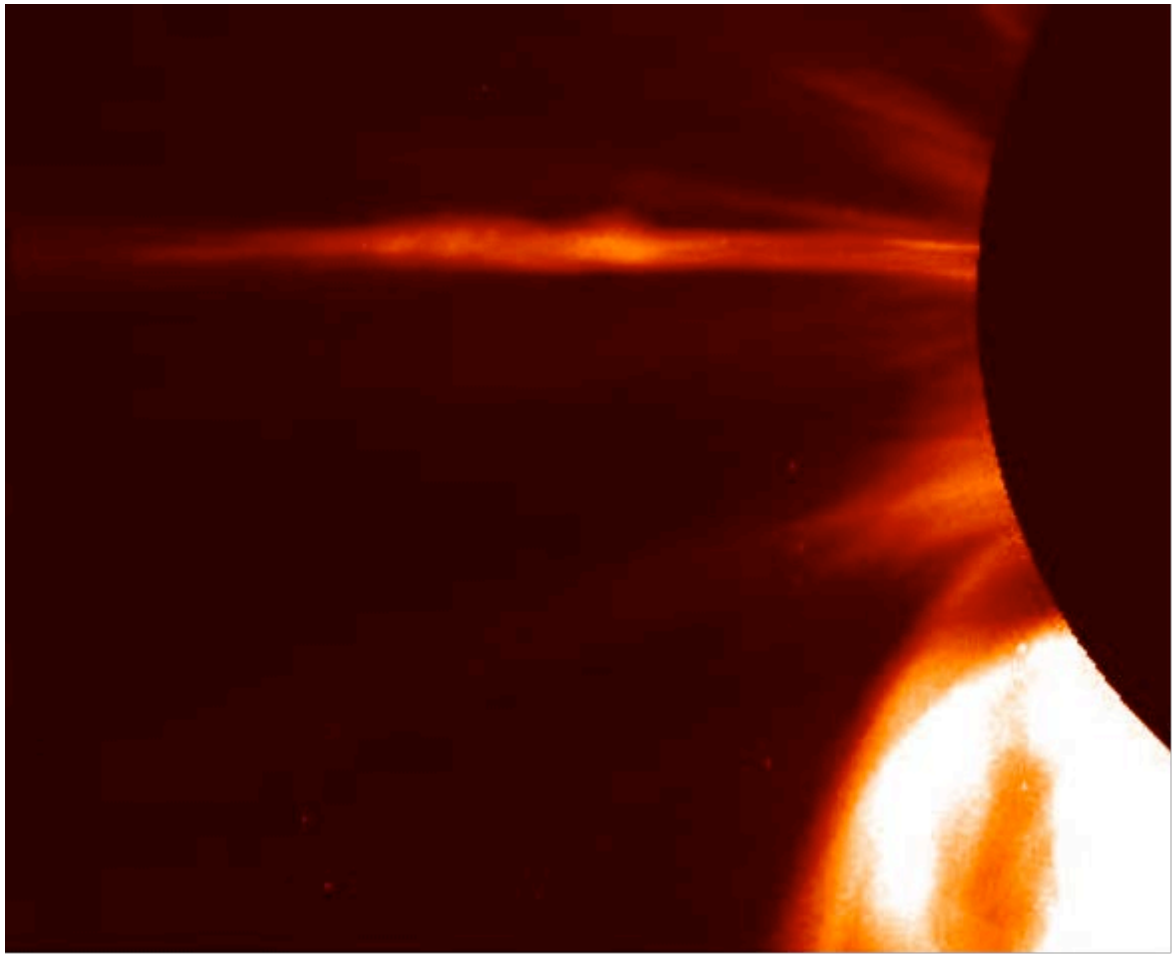

Courtesy: Lijia Guo

Turbulent Region Broadens as Instabilities Evolve

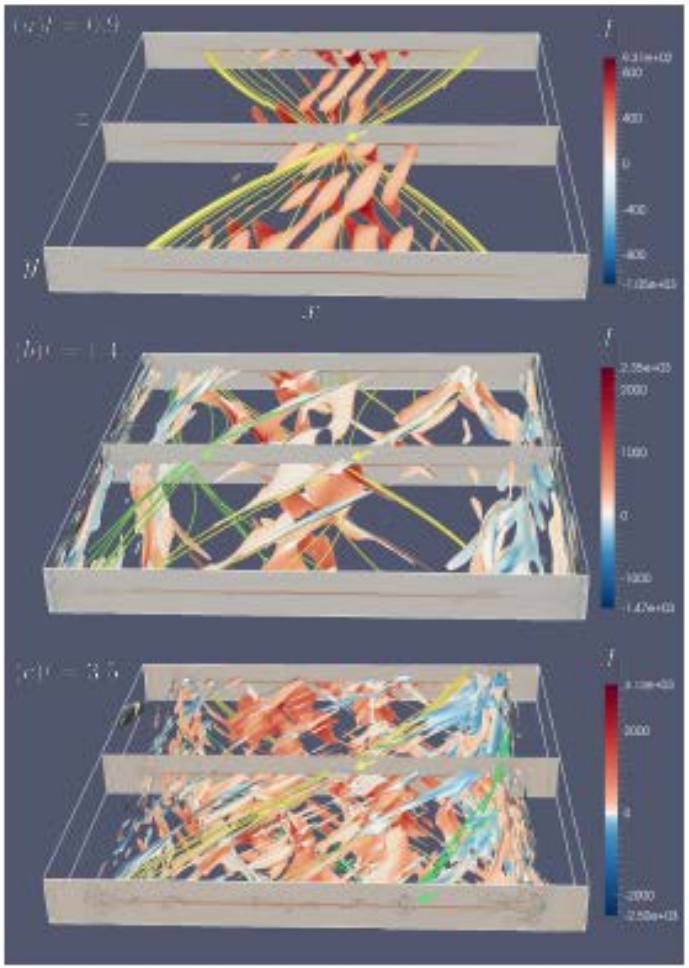

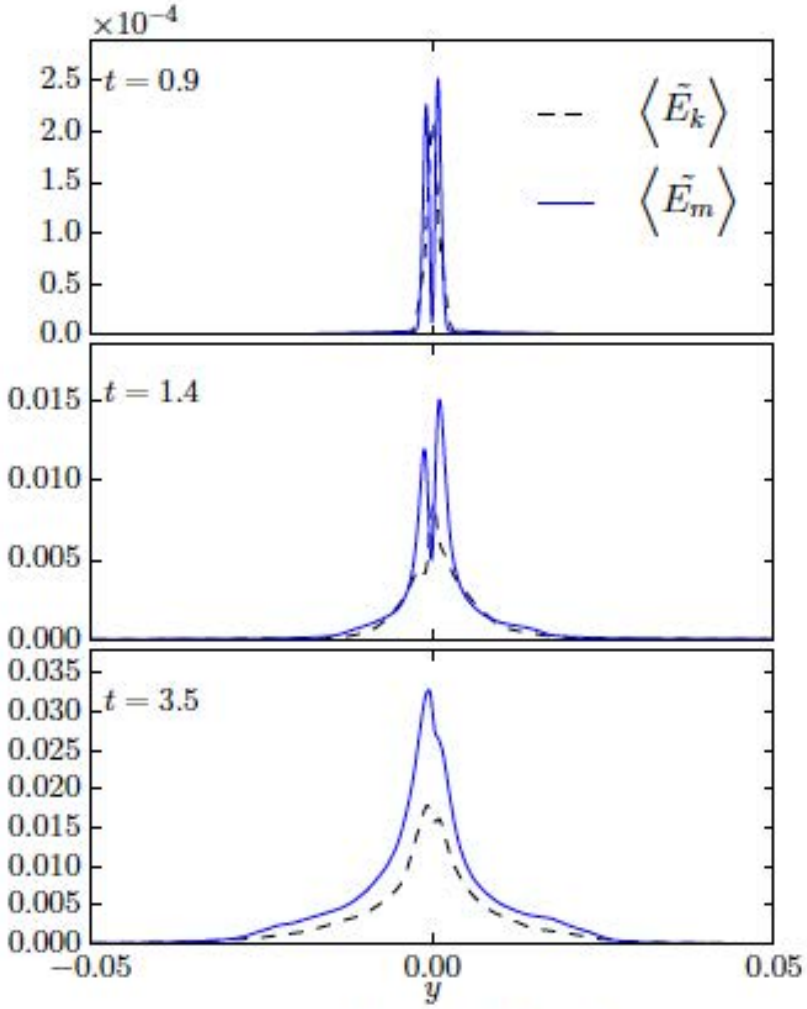

- In fully developed turbulent state, approximately 70% of turbulence energy is in $y = [-0.01, 0.01]$.

Plasmoid-Induced Turbulent Reconnection

$x - y$ slice of J_z at $z = 0$

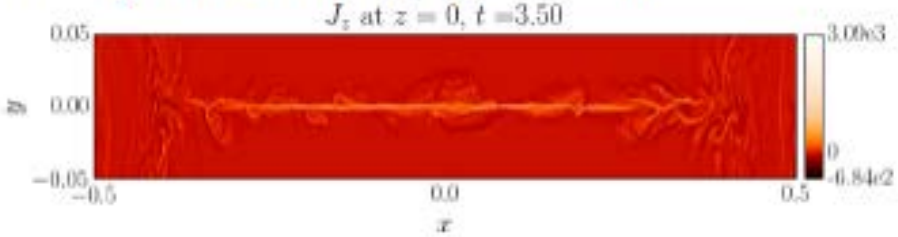

Mean field of outflow $\bar{u}_x$

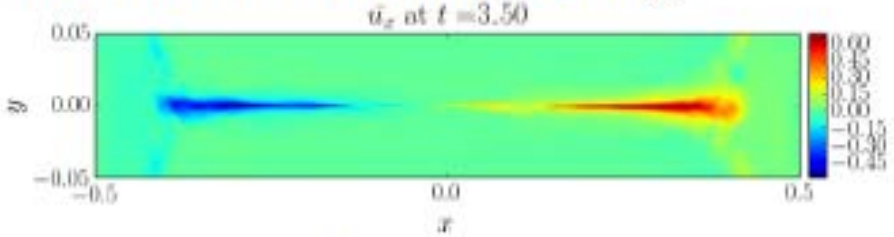

$x - z$ slice of J_z at $y = 0$

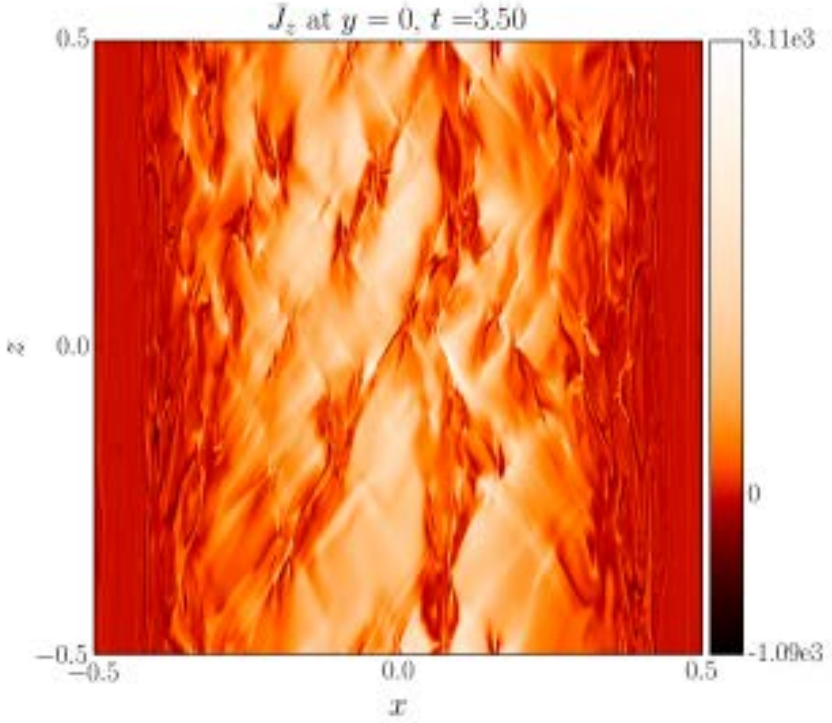

$x - z$ slice of u_x at $y = 0$

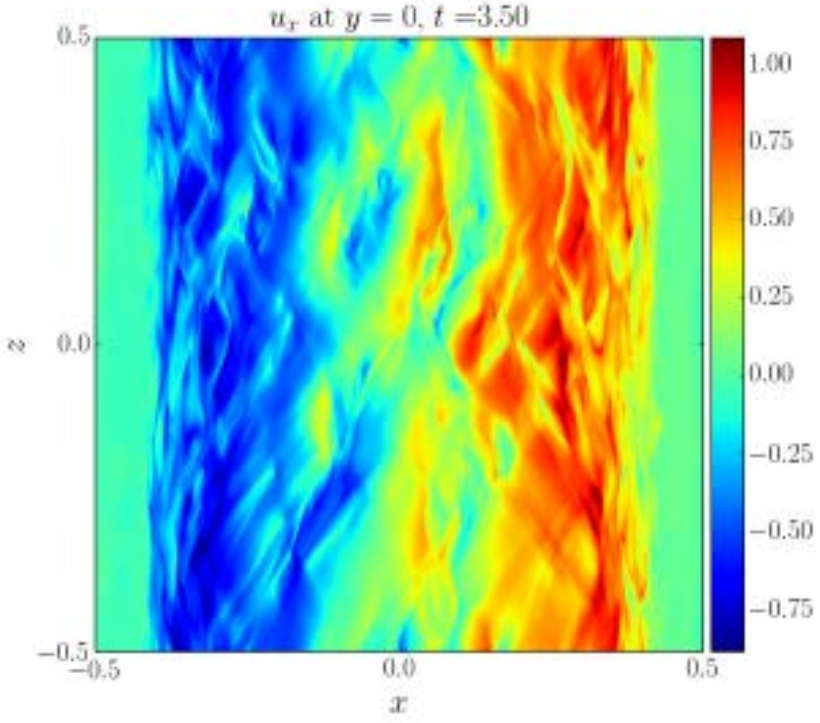

Reconnection Rate Comparison

- 2D and 3D plasmoid-dominated reconnection achieve comparable, faster than Sweet-Parker, reconnection rate
- 3D reconnection is measured with the mean field $\bar{\mathbf{B}} \equiv \frac{1}{L_z} \int \mathbf{B} dz$.

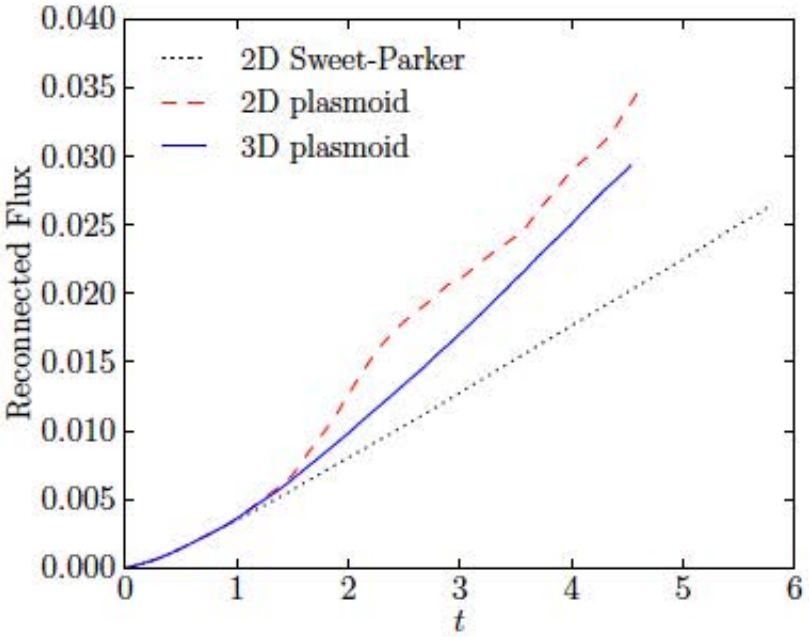

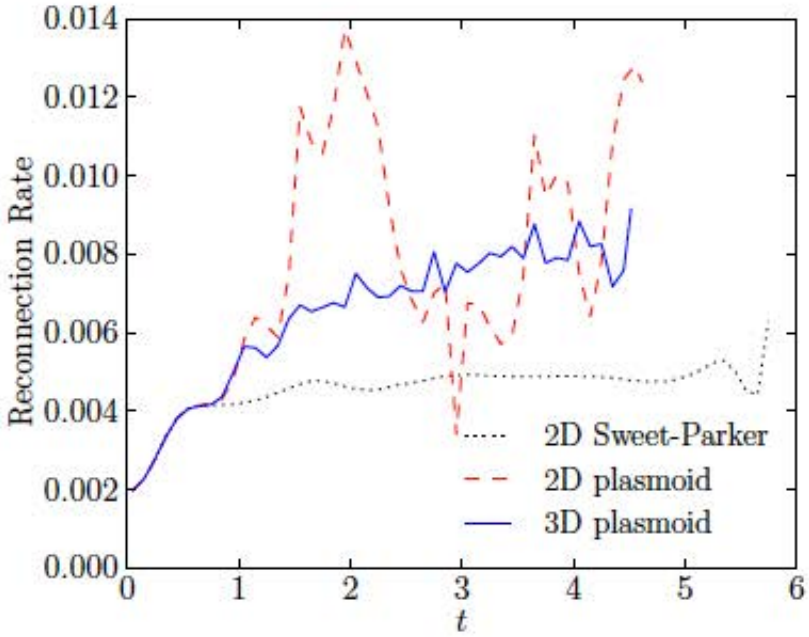

Outflow Profile Comparison

- 3D mean flow is similar to "blurred" Sweet-Parker
- Turbulent reconnection enhance reconnection rate by broadening the outflow jets

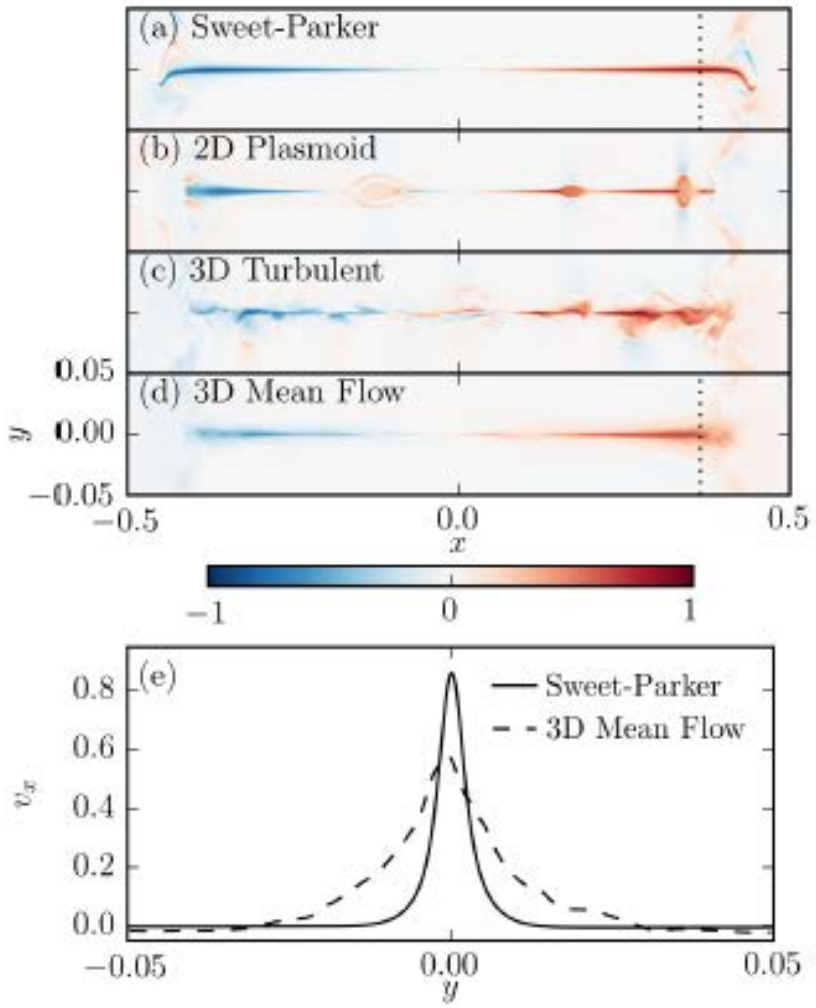

Spectra of Energy Fluctuations

- Integrated over y in $[-0.05, 0.05]$
- Mostly lie in the regions where $|k_x| \gtrsim |k_z|$ as dictated by $\mathbf{k} \cdot \mathbf{B} \simeq 0$

- 1D spectra are obtained by integrating azimuthally
- Energy spectrum $\sim k^{-\alpha}$
  $2.1 < \alpha < 2.3$ for $\tilde{E}_m$
  $2.3 < \alpha < 2.5$ for $\tilde{E}_k$

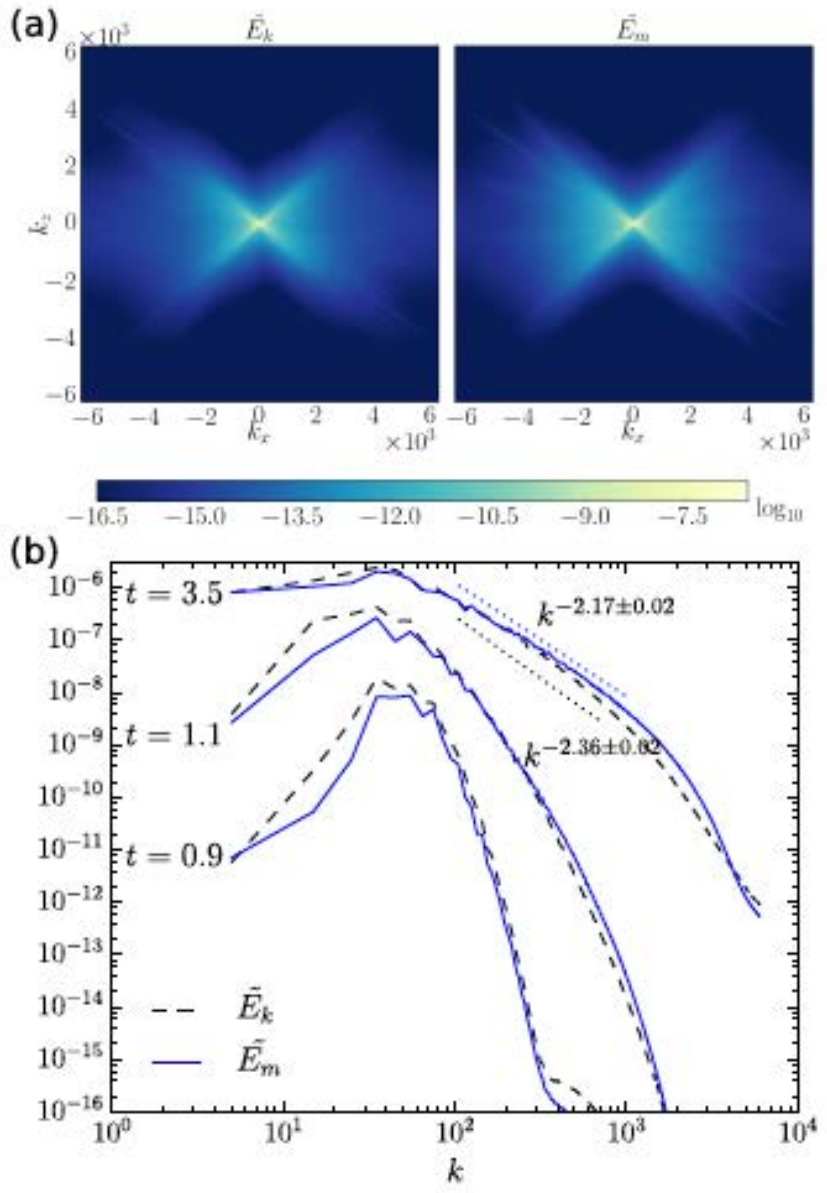

Role of the plasmoid instability in MHD turbulence

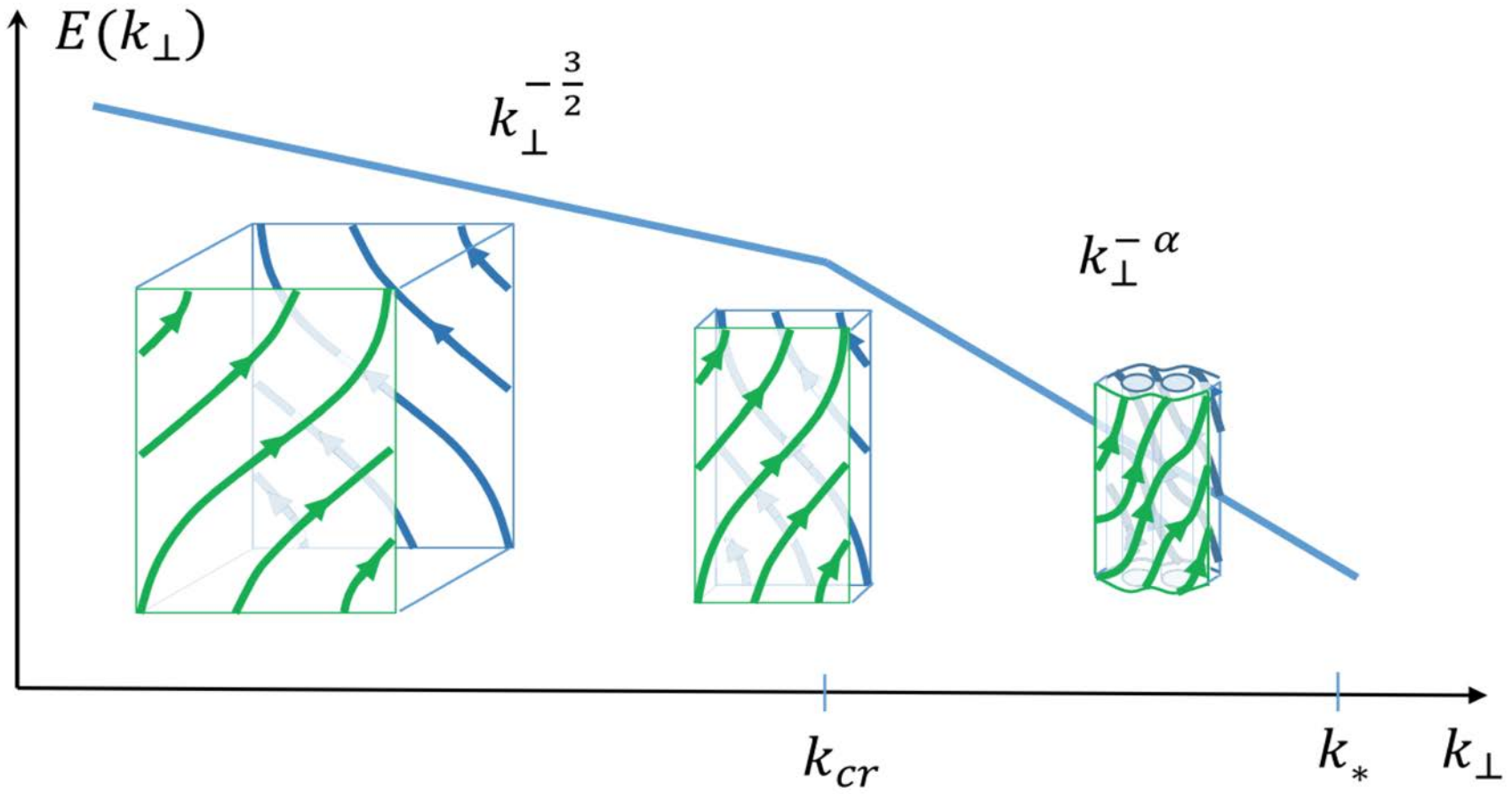

- Analytic theory predicts that the plasmoid instability can modify the turbulent energy spectrum (Carbone et al., 1990, Loureiro et al., 2017; Boldyrev and Loureiro, 2017; Mallet et al., 2017; Comisso et al., 2018)

Direct numerical simulation with $R_m=10^6$ (64000x64000 grids)

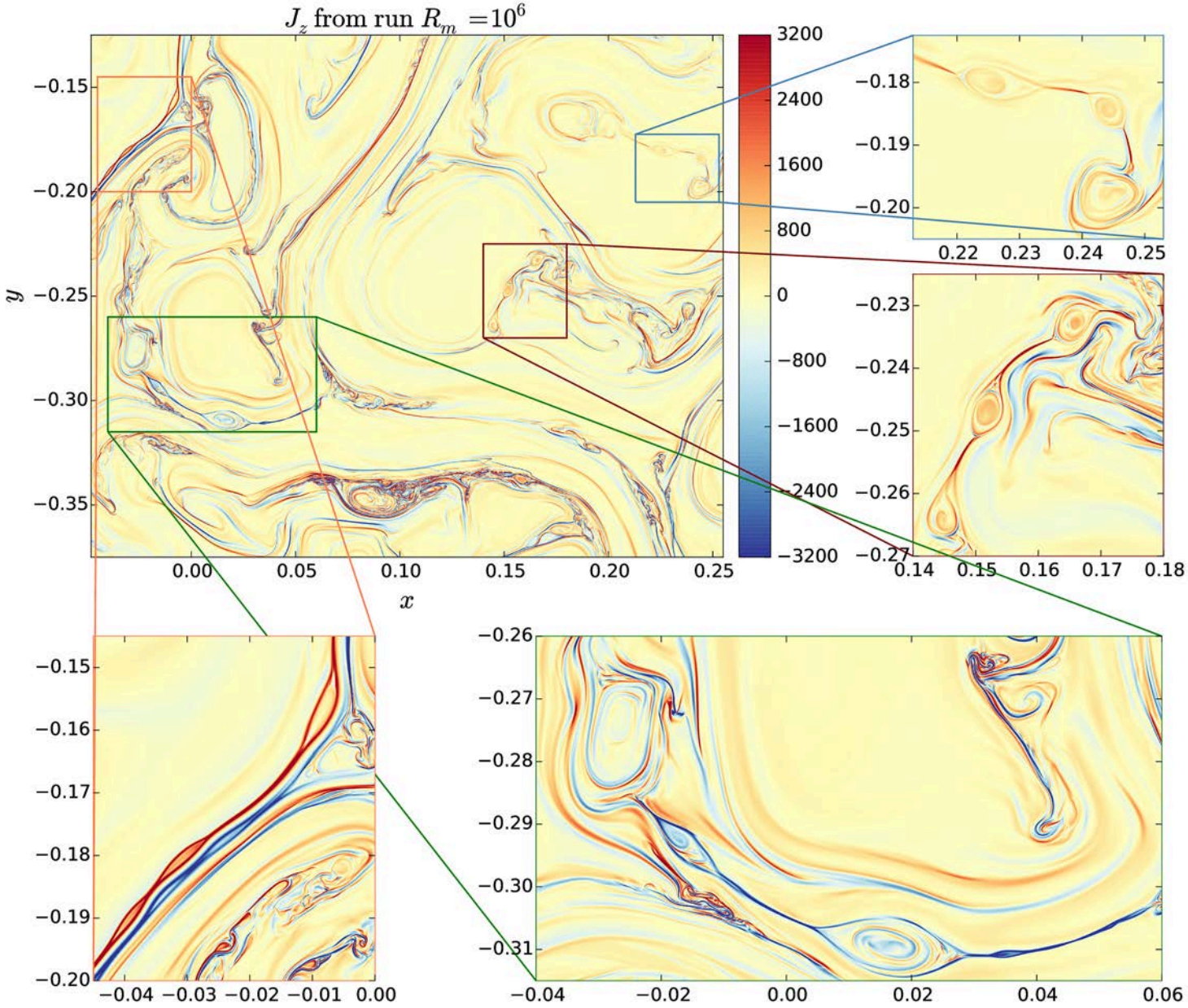

Direct numerical simulation with $R_m=8\times10^4$ (64000x64000 grids)

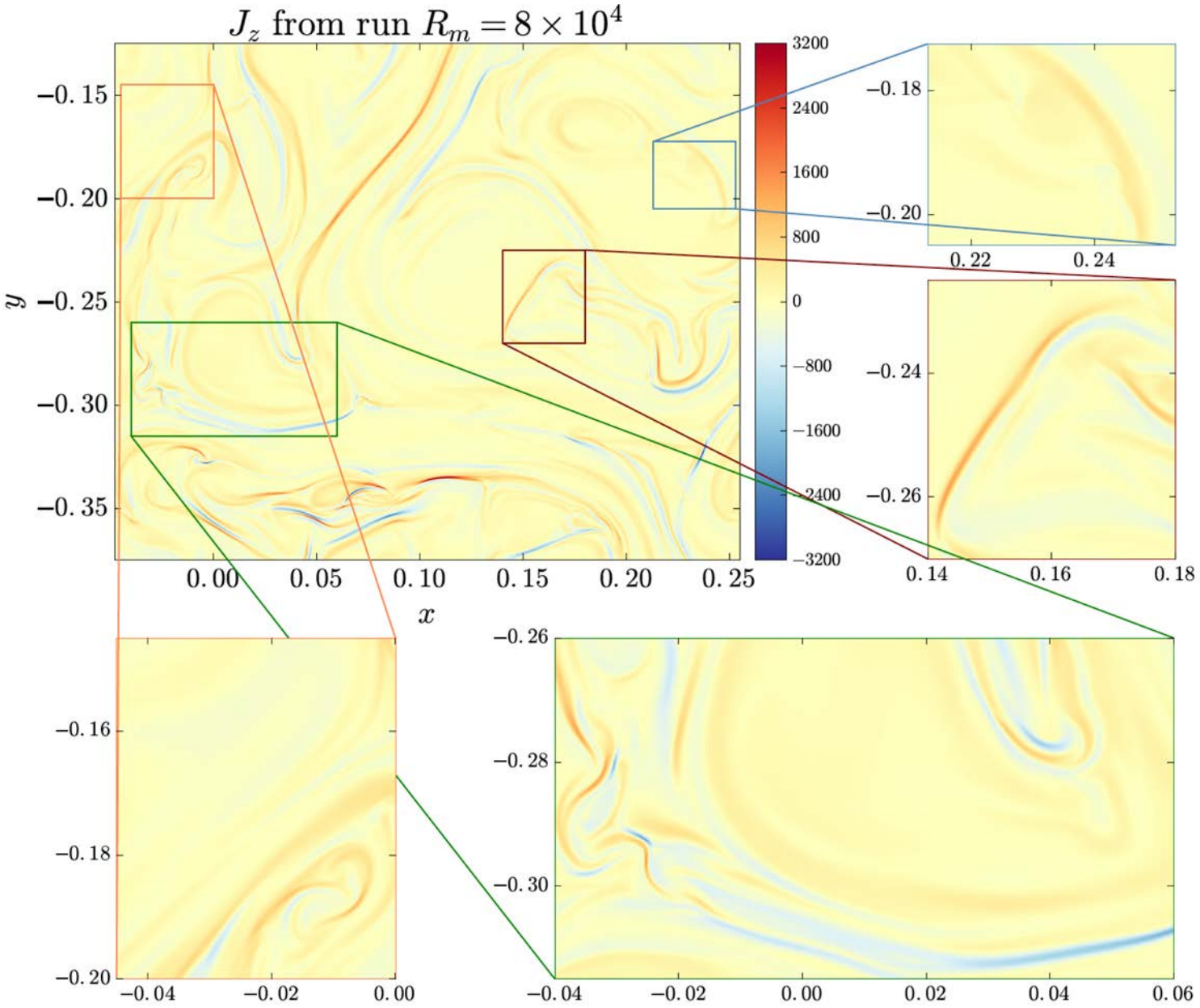

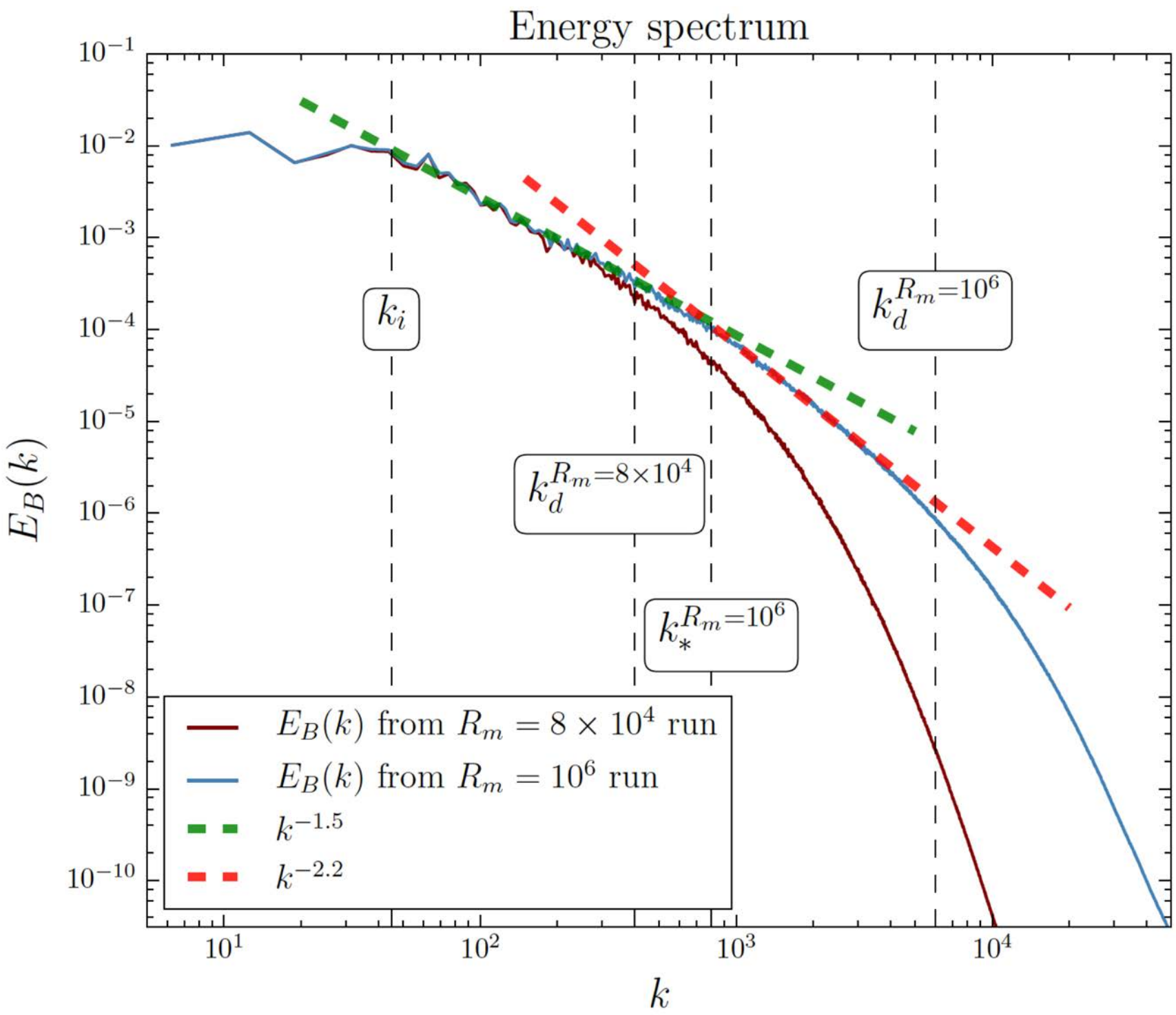
Energy spectrum
$E_B(k)$
k
k_i
$k_d^{R_m=10^6}$
$k_d^{R_m=8\times10^4}$
$k_*^{R_m=10^6}$
$E_B(k)$ from $R_m = 8 \times 10^4$ run
$E_B(k)$ from $R_m = 10^6$ run
$k^{-1.5}$
$k^{-2.2}$
10^{-1}
10^{-2}
10^{-3}
10^{-4}
10^{-5}
10^{-6}
10^{-7}
10^{-8}
10^{-9}
10^{-10}
10^1
10^2
10^3
10^4

Magnetic Reconnection: Sisyphus of the Plasma Universe

Titian, 1549

"The struggle itself …is enough to fill a man's heart. One must imagine Sisyphus happy."
---Albert Camus in *The Myth of Sisyphus (Le Myth de Sisyphe, 1942)*